공학박사학위논문

Guidance Laws to Control Impact Angle and Time for Missiles with Field-of-View Constraint

시야 제한이 있는 유도탄의 충돌각 및 충돌시간 제어 유도 법칙

2018년 8월

서울대학교 대학원
기계항공공학부
김 형 근

시야 제한이 있는 유도탄의 충돌각 및 충돌시간 제어 유도 법칙

Guidance Laws to Control Impact Angle and Time for Missiles with Field-of-View Constraint

지도교수 김 현 진

이 논문을 공학박사 학위논문으로 제출함

2018 년 6 월

서울대학교 대학원

기계항공공학부

김 형 근

김형근의 공학박사 학위논문을 인준함

2018 년 7 월

위 원 장 : 김 유 단

부위원장 : 김 현 진

위 원 : 박 민 지

위 원 : 전 명 윤

위 원 : 우 창 정

Guidance Laws to Control Impact Angle and Time for Missiles with Field-of-View Constraint

A Dissertation

by

HYEONG-GEUN KIM

Presented to the Faculty of the Graduate School of

Seoul National University

in Partial Fulfillment

of the Requirements

for the Degree of

DOCTOR OF PHILOSOPHY

Department of Mechanical and Aerospace Engineering

Seoul National University

Supervisor : Professor H. Jin Kim

AUGUST 2018

Guidance Laws to Control Impact Angle and Time for Missiles with Field-of-View Constraint

HYEONG-GEUN KIM

Department of Mechanical and Aerospace Engineering

Seoul National University

APPROVED:

Youdan Kim, Chair, Ph.D.

H. Jin Kim, Ph.D.

Min-Jea Tahk, Ph.D.

Byung-Eul Jun, Ph.D.

Chang-Kyung Ryoo, Ph.D.

to my

FAMILY and J

with love

Abstract

Guidance Laws to Control Impact Angle and Time for Missiles with Field-of-View Constraint

Hyeong-Geun Kim
Department of Mechanical and Aerospace Engineering
The Graduate School
Seoul National University

Homing guidance aims at guiding a missile to its intended target using information acquired from an on-board seeker. In real applications of homing guidance laws, a field-of-view restriction of the missile seeker is a significant issue because maintaining the seeker lock-on condition is an important task for acquiring the target information. Especially, when implementing advanced guidance laws to impose terminal constraints on impact angle and time, considering the field-of-view constraint is particularly essential since the curved trajectory may let the seeker's look angle exceed the confined field-of-view limit.

This dissertation presents guidance laws whose contributions are classified into three parts: *i*) impact angle control guidance law with the field-of-view constraint, *ii*) impact time control guidance law with the field-of-view constraint, and *iii*) impact angle and time control guidance law with the field-of-view constraint.

First, an impact angle control guidance law that confines the missile look angle during homing in order not to exceed a seeker's field-of-view limit is proposed. A sliding surface variable whose regulation guarantees the interception of a stationary target at the desired impact angle is designed, and the guidance law is derived to make the surface variable go to the sliding mode. Using a magnitude-limited sigmoid function in the surface variable, the proposed law prohibits the look angle from exceeding the specified limit during the entire homing. This capability to confine the missile look angle is valuable when a seeker's field-of-view is restricted, since imposing the terminal impact angle constraint demands the

missile to fly a curved trajectory. Furthermore, the proposed law only needs the line-of-sight angle and look angle among the target information. Thus, the proposed law can easily be implemented into a homing missile equipped with a structurally simple passive strapdown seeker. Theoretical analysis in this part indicates that the proposed law accomplishes the impact angle constraint without violating the look angle limit although it only uses the information of bearing angles.

Second, a guidance law that achieves the desired impact time without violating the seeker's field-of-view limit is presented. For the development of the law, kinematic conditions for impact time control are defined, and the backstepping control-based approach is adopted for the satisfaction of the conditions. The missile look angle is utilized as a virtual control input for the backstepping structure, and its magnitude is limited by a prescribed limit by restricting the controller gain. Consequently, the impact time constraint can be achieved with satisfying the look angle limit under the proposed law. Since few papers considering the field-of-view limit under the impact time control are available in open literature, the capability to confine the seeker's look angle with achieving the desired impact time is the main contribution of this part.

Finally, a guidance law for impact angle and time control with taking into account the field-of-view constraint is developed. Basically, the law in this part is formed as a look angle-limited impact angle control guidance law that has an additional guidance gain. Since the length of the trajectory under this law is calculated as a function of this gain, the terminal impact time can be controlled by adjusting the gain. As a result, the proposed guidance law in this part can intercept the stationary target at the desired impact angle and time with satisfying the field-of-view limit. The proposed law is expected to achieve the accurate performance in real applications owing to its closed-loop structure without using any numerical routine such as off-line optimization or the shooting method.

To evaluate the performance of the proposed laws, numerical simulations are conducted for each part. The results demonstrate that the proposed laws accomplish the desired terminal tasks with preventing the look angle from exceeding the prescribed limit.

Keywords: Homing guidance, Field-of-view limit, Impact angle control, Impact time control

Student Number: 2014-30356

Table of Contents

List of Tables

List of Figures

1 Introduction

1.1 Background and motivations

The deployment of precision-guided munitions (PGM) is essential in modern warfare in order to augment lethality against enemy forces and minimize collateral damage. Guided missiles are the most representative PGM, and have been utilized for a great deal of warfare since its development in World War II. For an accuracy of the guidance, a manner of guiding the missile to the intended target, referred to as missile guidance, is necessary. Especially, as the missile approaches the target, a guidance method called homing guidance where the missile with on-board seeker autonomously yields the command to its own control surface is effective in improving the measurement accuracy.

Proportional navigation (PN) guidance, given the primary objective of the missile is to intercept the target with zero miss distance, has been widely used as one of the well-known homing guidance [1]. PN guidance is based on the property that the pursuer maintaining a constant line-of-sight (LOS) is on the collision path against the target. Thus, simply structured to nullify the LOS rate with a proportional gain called navigation constant,

PN guidance is able to achieve the interception. Furthermore, PN guidance with a navigation constant of three has optimality for minimizing the steering energy and terminal miss distance against the stationary target [2]. Namely, PN guidance yields satisfactory performance with the simplicity in implementation.

Advances in anti-air defense systems, such as close-in weapon system (CIWS) or electronic countermeasure (ECM), pose a great challenge in increasing lethality and survivability of the homing guided missiles. Simple PN guidance with a fixed navigation constant is insufficient for overcoming the defense systems since its only goal is to nullify the zero effort miss. In this regard, to enable the execution of an additional task for incapacitating the defensive system of the target becomes an important issue.

To impose terminal constraints such as impact angle and time would be an effective solution against the defensive system. Control of the impact angle enables the missile to select the desired collision way at the terminal stage of the homing so that the destruction to the weak point of the armored target can be fulfilled. Imposing the impact time constraint can also be a useful strategy because it facilitates a salvo attack in which multiple missiles attack the same target simultaneously. Since the self-defensive system on the ship is limited in the number of missiles it can defend simultaneously, the survivability of each missile is enhanced. For these reasons, there have been plenty of studies about impact angle control guidance [3–22] and impact time control guidance [23–34]. Much research on the guidance laws that involve both impact angle and time constraint is also available in open literature [35–40].

For the successful homing guidance, the seeker's lock-on to the target should be maintained until the interception because the guidance state information is acquired from the on-board seeker. Under PN guidance, the seeker look angle continually decreases as the missile approaches the stationary target since the LOS rate is forced to be nullified, so there is no need to seriously consider the maintenance of the lock-on condition.

On the contrary, the implementation of advanced guidance laws involving impact angle and time constraints requires the careful consideration of the seeker's field-of-view (FOV)

limit because the curved trajectory may let the seeker's look angle exceed the confined FOV limit. In particular, when the missile is equipped with a strapdown seeker which has a narrow FOV compared with a gimbal seeker, this consideration is an essential task in terms of maintaining the seeker lock-on condition. As a result, for the successful homing guidance against targets having defensive systems, it is effective to develop guidance laws that takes into account the FOV limit with terminal constraints such as impact angle and time.

1.2 Literature survey

In this section, the survey of books, papers, and other resources associated with this research is presented. The related studies are classified into the following three parts considering the subjects of this dissertation: *i*) impact angle control guidance, *ii*) impact time control guidance, *iii*) impact angle and time control guidance.

1.2.1 Impact angle control guidance

Fulfillment of the impact angle is a significant requirement for land-attack or anti-ship missiles because it allows the missile to attack the weak point of an armored target by adjusting the collision direction. For anti-air missiles, imposing the impact angle constraint would also be an effective strategy owing to its capability to determine the collision geometry. Over the past few decades, many guidance laws that impose the terminal impact angle have been developed by virtue of these advantages since the first attempt in [3]. Particularly, various recent studies about impact angle control guidance focuses practical issues such as limited field-of-view (FOV) constraint or restriction of available target information. In accordance with the main topic of this dissertation, FOV-constrained guidance laws, the survey of this subsection also concentrates on the impact angle control guidance laws considering FOV limit.

The previous works about impact angle control guidance considering the confined FOV

limit can be classified into two categories of methods based on linearized dynamics [12–15] and nonlinear approaches [16–20]. In common linear methods, the guidance law is designed as a polynomial form of time-to-go or relative range. In [12], a guidance law made up of time-to-go polynomial is developed in order to achieve the desired impact angle with zero terminal command. With linearization of the flight path angle, the entire look angle profile of the closed-loop under the law in [12] is obtained as a polynomial form, which enables the user to modulate the maximum magnitude of missile look angle by adjusting a set of gains in advance. A guidance law in [13] is formulated as a sum of the time-to-go polynomial guidance command of [12] and an additional term proportional to the cross range. In this way, the homing missile moves with an oscillatory trajectory normal to the desired collision course, which allows the target observability to be enhanced compared with the conventional time-to-go polynomial guidance. Like the work in [12], adjusting the polynomial gains beforehand also enables to confine the maximum missile look angle [13].

Unlike the laws in [12] and [13] explained above, which pre-calculate the maximum magnitude of the look angle based on the closed-loop trajectory solution, a guidance law in [14] directly handles the look angle constraint during the homing phase by adopting the optimal control theory. Utilizing the optimal control theory considering the inequality constraint of the state variable given by [41], the law in [14] can prevent the seeker look angle from exceeding the prescribed value. As an advanced version of the work in [14], a range-to-go weighted optimal guidance law is developed in [15]. Similar to [14], the optimal control theory is applied considering the state variable inequality constraint in order to fulfill the impact angle control guidance without violating the FOV limit. The range-to-go is additionally multiplied in the performance index of the control energy, so the terminal command converges to zero unlike the law in [14].

The laws in [12–15] mentioned above, derived based on the linearized engagement kinematics, require the knowledge of the relative range between the missile and target because all these laws are expressed as functions of time-to-go or range-to-go. When the missile system is equipped with a passive sensor such as an infrared seeker or a passive sonar,

however, the range information is difficult to measure in real time. In this regard, several nonlinear guidance laws utilizing the characteristics of the pure proportional navigation (PPN) guidance or biased pure proportional navigation (BPPN) guidance which does not require the accurate measurement of the relative range have been proposed.

Multi-phase composite guidance scheme, whose capability to control the terminal impact angle is studied by the authors in [21] and [22], switches the navigation constant or biased term during the homing in order to achieve the desired tasks. Based on this multi-phase structure, several impact angle control guidance laws involving the FOV constraint are addressed. The authors in [16] propose a two-phase guidance scheme composed of the PPN guidance and BPPN guidance. Since the closed-loop solution under the two-phase law is obtained in this paper, the desired duties of satisfying the terminal impact angle without violating the look angle limitation can be accomplished by adjusting the integral of the bias profile. However, a selection of the bias profile is proceeded by trial and error in order not to violate the limited FOV condition because a specific condition for limiting the look angle is not given analytically in this work. As an improved version of the law in [16], two types of laws, i.e. switched-gain PPN (SGPPN) and switched-bias PPN (SBPPN), are designed in [17]. These two laws provide specified conditions that guarantee the satisfaction of the look angle constraint, so the desired tasks can be achieved more readily compared with the law in [16]. The study in [18] deals with not only the look angle constraint but also the acceleration command limitation by developing a BPPN guidance law that switches the bias term. The designed BPPN law with the navigation constant of $N > 2$ also achieves zero terminal command since the bias term converges to zero at the terminal stage. The work in [19] proposes a look angle constrained guidance law that considers the limited acceleration constraint. Similar to the works in [16] and [17], the navigation gains for satisfying the desired constraints are calculated by numerical solving. By the fact that the PPN with $N = 1$ maintains the look angle as a constant, the switched-gain PPN law in [20] satisfies the constraints on the impact angle and look angle with a change of the navigation constant from $N = 1$ to $N = N_s \geq 2$.

The above composite guidance laws in [16–18, 20] except for [19] do not involve the range information in their command. Although the law in [19] requires the knowledge of relative range for embodying the switching scheme, the measurement of the range is not necessary for its implementation since an observer estimating the range is also developed with the guidance law. Therefore, the laws in [16–20] are useful when the guided system is equipped with a passive sensor or jammed by an electronic attack such as an electronic countermeasure (ECM) because the range information is not required.

1.2.2 Impact time control guidance

The impact time control is an effective strategy, for it facilitates a salvo attack where multiple missiles attack the same target simultaneously. Since the self-defensive system on the ship is limited in the number of missiles it can defend simultaneously, the survivability of each missile is enhanced in salvo attack. That is, control of the impact time when employing multi missiles can allow lethal attack despite the presence of the anti-air defensive system.

One of the initial efforts that assign the impact time constraint to the missile guidance law is given by [23]. The authors of [23] formulate the linearized suboptimal problem constrained by the terminal miss distance and desired impact time. The closed-form solution of the proposed problem, which is utilized as the guidance command, is obtained as a combination of PN guidance law and the feedback term that aims to regulate the impact time error. In [24], a cooperative PN-based guidance law using time-varying navigation gain is designed. The proposed law conjugates a concept of time-to-go variance, thereby enabling multiple missiles to perform many-to-one engagement without specified desired impact time. The laws in [23] and [24] are derived based on the linearized engagement dynamics with the small angle assumption. The accuracy of such guidance laws can be deteriorate under the presence of influential nonlinearity such as large heading error.

The authors of [25–30] design impact time control guidance laws based on the nonlinear engagement dynamics for ensuring the performance under diverse engagements. The guidance laws in [25–28] fulfill the impact time control by letting the estimated time-

to-go converge to the desired time-to-go. These laws can guarantee a wide range of the capture region with an acceptable command in virtue of their exact formulation without linearizations. Especially, the laws in [26] and [27] are extended to engagements involving a non-stationary and non-maneuvering target using the concept of the predicted interception point (PIP) method first represented in [26]. In [29], an expected impact time is accurately calculated using the beta function, and a guidance law is developed to make the expected impact time equal to the desired impact time. Expressions of the achievable minimum and maximum impact times are also derived based on the analysis of the proposed law. The work in [30] combines the PN guidance law and a feedforward control term composed of the impact time error based on nonlinear formulation. Similar to [26] and [27], the law in [30] is also extended to a non-stationary moving target utilizing the PIP technique.

Taking advantage of the explained impact time control guidance laws allows the multiple missiles to carry out a salvo attack that can incapacitate the defensive system of the target. In the implementation, however, there is the possibility that the missile loses the target from the seeker's FOV since imposing the impact time constraint may give rise to the curved trajectory of the missile. Therefore, an impact time control guidance law that considers the seeker's FOV limit is required from the implementation point of view. There are some studies that consider the FOV limit as well as the impact time constraint [31–34].

In [31], a switching logic that keeps the missile look angle within the maximum limit is proposed. Applying this logic to the impact time control guidance law of [23], the guidance scheme developed in [31] can prevent the look angle from exceeding the seeker's FOV limit. However, the switching logic-based law brings about a sudden change in its guidance command, which is undesirable from a practical point of view. To overcome this drawback, the authors in [32] and [33] utilize a continuous cosine-based function to limit the look angle without using the switching logic. Especially, the law presented in [33] can keep the look angle from violating the maximum FOV limit in the presence of uncertain autopilot lag. In [34], an impact time control guidance law that ensures the monotonic decrease of the look angle is proposed. Thereby, the look angle does not exceed the initial value during

the entire homing phase, so the constraint on FOV is also satisfied by letting the initial look angle be within the maximum bounds.

1.2.3 Impact angle and time control guidance

A salvo attack with fulfilling the impact angle control enhances effectiveness of the cooperation since each missile can aim at weak parts of the target. It also prevents from the missiles colliding each other owing to the capability to adjust the collision directions. Despite these advantages of controlling the impact angle and time simultaneously, there are not many related studies while much research that only considers the impact angle or impact time is available in open literature.

One of the pioneering works that involve the terminal impact angle and time constraint is addressed in [35]. In this work, an impact angle control law is designed based on the optimal control theory and extended into an impact angle and time control law by using a time-to-go estimation. The guidance law proposed in [36] is a downrange-based polynomial function with three coefficients. The coefficients are calculated to satisfy the desired terminal constraints: zero miss distance, desired impact angle, and desired impact time. The laws in [35] and [36] are designed based on the linearized engagement dynamics under the small angle assumption of the missile flight path angle. Although the linearization makes it easier to derive and analyze the guidance laws, the performance of such guidance laws can be degraded in the engagement situations when it is difficult to apply the small angle assumption.

To guarantee the guidance performance under various engagement situations, other guidance laws derived from nonlinear engagement dynamics have been proposed. In [37], sliding mode control (SMC) is used for deriving the guidance law against a non-stationary target. The impact angle is constrained by tracking the desired LOS angle using second-order SMC. The profile of the desired LOS angle involves the extra parameter which is tuned to satisfy the impact time constraint through off-line optimization. The authors in [38] propose the optimal guidance law to satisfy the impact angle and time constraints.

The guidance law is derived by solving a two-point boundary value problem (TPBVP) with constraints based on a nonlinear engagement kinematics. PN-based guidance laws presented in [39] takes into account a practical requirement such as FOV and acceleration limit as well as the impact angle and time constraints. The guidance parameters for achieving the designated tasks are found by a numerical routine. The laws in [37–39] satisfies a wide range of the capture region owing to their capability to handle nonlinearity. For the implementation, however, an optimization routine is required, which demands longer computation time in comparison with the analytic approaches.

1.3 Research objectives and contributions

This dissertation proposes field-of-view constrained guidance laws whose contributions are divided into three parts: *i*) impact angle control guidance law, *ii*) impact time control guidance law, *iii*) impact angle and time control guidance law. In this section, the research objectives and contributions of each part are described.

1.3.1 Impact angle control guidance law with field-of-view constraint

This part proposes an impact angle control guidance law that restricts the seeker look angle within the prescribed limits. The proposed law is designed to be implemented under bearings-only measurements, which means that the produced command does not involve any information of the relative range and LOS rate. Compared with the previously published studies related to the impact angle control considering the FOV constraint in [12–20], the proposed work in this study has the following contributions. First, the developed law does not demand any knowledge of the time-to-go or relative range unlike the existing linear methods in [12–15]. Therefore, the proposed law can easily be implemented onto a missile equipped with a passive seeker. Furthermore, the proposed law does not involve the LOS rate information unlike the existing PN-based nonlinear approaches in [16–20]. That

is, just bearings-only measurement without estimating the relative range or LOS rate is enough for the implementation of the proposed guidance law, so it provides advantages of jamming avoidance and low development cost by allowing a structurally simple sensor such as a strapdown passive seeker. In addition, the application of the proposed law does not require numerical computation during the entire homing unlike several laws in recent studies [14,15,17,19]. Thus, an issue of performance reduction caused by lack of calculation time or capacity needs not be considered when employing the guidance law. Analytic proofs and numerical simulations for the proposed law are also included in this part. The results demonstrate that the proposed law accomplishes the impact angle constraint without violating the maximum look angle limit although it only uses the information of bearing angles.

1.3.2 Impact time control guidance law with field-of-view constraint

An impact time control guidance law considering the missile seeker's FOV limit is presented. Two error variables, which aim to achieve the homing and impact time control respectively, are introduced, and the guidance law is derived by regulating the defined variables based on backstepping control. The proposed law utilizes a missile look angle as a virtual control input of the backstepping structure. The law is designed to restrict the magnitude of the missile look angle by confining the virtual controller's gain, thereby satisfying the limited FOV condition. Here, since the virtual look angle is designed as a continuously differentiable function, the derived guidance law can prevent the violation of the FOV limit without using discrete switching logic unlike the approach in [31]. In addition, minimum and maximum impact times that can be achieved sufficiently by the proposed law is investigated. By theoretically proving that the developed law can satisfy any impact time between the calculated minimum and maximum bounds, the analysis of the achievable impact time in this part provides a meaningful discussion for the implementation. Numerical simulations

against a stationary target are carried out, and the result demonstrates the validity of the proposed guidance law.

1.3.3 Impact angle and time control guidance law with field-of-view constraint

A guidance law that considers the field-of-view limit as well as the terminal impact angle and time constraint is proposed. Prior to dealing with both the impact angle and time constraints, a look angle constrained guidance law that only involves the impact angle constraint is firstly designed. Since the remaining trajectory under this law is formulated as a function of a gain used in the guidance command, the time-to-go until the interception is adjustable. Therefore, the developed impact angle control guidance law can also control the terminal impact time. The proposed law can also prevent the look angle from exceeding the maximum FOV, which is not considered in almost recent studies [35–38]. Since imposing the impact angle and time constraints brings about the curved trajectory, this capability to confine the look angle is valuable. Furthermore, the proposed law is derived without requiring the small angle assumption of the flight path angle unlike the existing linear approaches in [35] and [36]. Hence, the guidance accuracy is ensured for various impact angles under the proposed law. Although the existing nonlinear methods in [37–39] can also achieve the accurate performance owing to their exact formulations without linearizations, numerical routine such as off-line optimization or shooting method is required for the application of these laws. On the contrary, the proposed law can be implemented without using any numerical routine, so more feasible for real applications in comparison with the laws in [37–39]. The effectiveness of the proposed guidance law is demonstrated by simulations.

1.4 Thesis organization

The remainder of this paper is composed of as follows. In Chapter 2, a look angle constrained impact angle control guidance law for homing missiles with bearings-only measurements is presented. In Chapter 3, an impact time control guidance law that also prohibits the look angle from exceeding the maximum limit is introduced. In Chapter 4, a guidance law that controls both the impact angle and time with satisfying field-of-view constraint is proposed. In Chapter 5, the primary results and contributions of this paper are summarized.

2

Impact Angle Control Guidance with Field-of-View Constraint

This chapter presents an impact angle control guidance law that confines the missile look angle during homing in order not to exceed a seeker's field-of-view limit. A sliding surface variable whose regulation guarantees the interception of a stationary target at the desired impact angle is designed, and the guidance law is derived to make the surface variable go to the sliding mode. Using a magnitude-limited sigmoid function in the surface variable, the proposed law prohibits the look angle from exceeding the specified limit during the entire homing. This capability to confine the missile look angle is valuable when a seeker's field-of-view is restricted, since imposing the terminal impact angle constraint demands the curved trajectory to the missile. Furthermore, the proposed law can be implemented under bearings-only measurements because the command does not involve any information of the relative range and line-of-sight rate. Numerical simulations are conducted to demonstrate the validity of the proposed law. The contents of this chapter are also available in the open literature of [42].

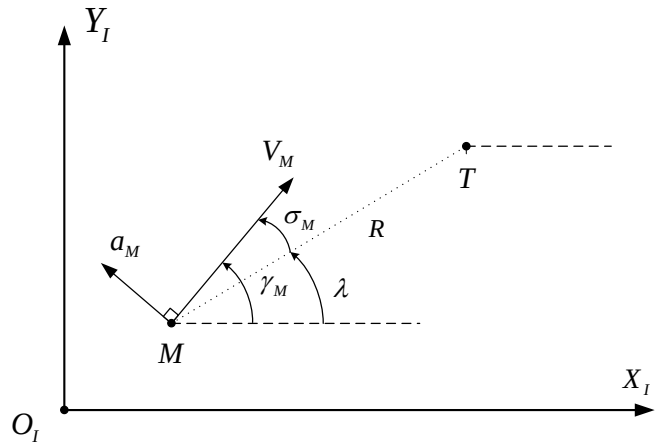

Figure 2.1: Two-dimensional engagement geometry for a stationary target

2.1 Problem statement

This section gives the nonlinear dynamics of the planar engagement against a stationary target to formulate the guidance problem for impact angle control. Figure 2.1 illustrates the two-dimensional geometry for the engagement between the missile and target denoted as M and T respectively. The frame $X_I O_I Y_I$ represents the inertial coordinate, and V_M, γ_M and a_M denote the speed, flight path angle and normal acceleration of the missile respectively. σ_M is the look angle defined as the angle between the LOS and missile heading under the assumption that the angle of attack is small enough to be neglected. R and λ mean the relative range and LOS (line-of-sight) angle between the missile and target. Based on the variables defined in Fig. 2.1, the governing equations are expressed as

$$\dot{R} = V_R \tag{2.1a}$$

$$R\dot{\lambda} = V_\lambda \tag{2.1b}$$

where V_R and V_λ represent the relative velocity component of the target to the missile along and perpendicular to the LOS respectively as

$$V_R = -V_M \cos \sigma_M \tag{2.2a}$$

$$V_\lambda = -V_M \sin \sigma_M. \tag{2.2b}$$

Since the normal acceleration a_M is applied to the missile velocity vector, the equation of the flight path angle is written as

$$\dot{\gamma}_M = \frac{a_M}{V_M} \tag{2.3}$$

The design objective of the guidance law is to intercept the target with the desired impact angle without violating the prescribed look angle limits, which is expressed mathematically as

$$R(t_f) = R_f \tag{2.4a}$$

$$\gamma_M(t_f) = \gamma_d \tag{2.4b}$$

$$|\sigma_M(t)| \leq \sigma_M^{\max} \leq \pi/2 \quad \forall t \in [0, t_f] \tag{2.4c}$$

where t_f, R_f, γ_d and $\sigma_M^{\max}$ are the final time, acceptable maximum miss distance, desired impact angle and prescribed look angle limit. Furthermore, the bearings-only measurement of the missile is assumed in this work. Therefore, the guidance law is designed to achieve the constraints in (2.4) using only the LOS angle and look angle without involving the LOS rate and relative range.

2.2 Design of impact angle control guidance law

This section introduces the kinematic conditions for achieving the impact angle control without violating the FOV constraint during the homing, and presents a sliding mode-based guidance law to satisfy the formulated conditions.

2.2.1 Kinematic conditions for impact angle control guidance

The collision path on which the missile moves toward the target along the LOS is achieved by nullifying the missile look angle as

$$\sigma_M = 0 \tag{2.5}$$

In addition, choosing the collision path whose direction is equal to the desired impact angle guarantees the satisfaction of impact angle constraint, which is equivalent to

$$\lambda = \gamma_d. \tag{2.6}$$

Therefore, fulfilling the both conditions (2.5) and (2.6) always ensures the interception at the desired impact angle, so the following surface variable is defined to achieve the desired tasks:

$$S\left(\sigma_M, \lambda\right) = e_2 - k_1 \mathrm{sgmf}(e_1, \phi_1) \tag{2.7}$$

where the variables e_1 and e_2 are introduced to satisfy the conditions in (2.5) and (2.6) as

$$e_1 = \lambda - \gamma_d \tag{2.8a}$$

$$e_2 = \sigma_M, \tag{2.8b}$$

and the sigmoid function sgmf$(\cdot)$ is defined as

$$\mathrm{sgmf}(x, \phi) = \frac{x}{\sqrt{x^2 + \phi^2}} \tag{2.9}$$

The user chosen parameters k_1 and ϕ_1 are constants such that

$$\begin{aligned} &0 < k_1 < \sigma_M^{\max} < \frac{\pi}{2} \\ &0 < \phi_1. \end{aligned} \tag{2.10}$$

Then, the regulation of the S defined in (2.7) yields

$$\begin{aligned} \frac{d}{dt}\left(\frac{1}{2}e_1^2\right)\bigg|_{S=0} =& e_1\dot{\lambda}\bigg|_{S=0} \\ =& -\frac{V_M}{R}e_1 \sin\left\{k_1 \mathrm{sgmf}(e_1, \phi_1)\right\} \\ <& 0 \quad \forall e_1 \in \mathbb{R} - \{0\} \end{aligned} \tag{2.11}$$

where the inequality (2.11) is obtained by the fact that $0 < k_1 \leq \pi/2$ from (2.10). Thus, the variable e_1 approaches zero, which also enables $e_2 \to 0$ from (2.7). Here, to guarantee the achievement of the desired conditions (2.5) and (2.6) indisputably, it should be additionally verified that e_1 goes to zero before homing is over. The analysis about this issue of finite time convergence is dealt with in section 2.3-C.

Also note that the proposed surface variable S consists only of the look angle and LOS angle. It accords with the design requirement to implement under the bearings-only measurement. From now on, we denote the surface variable as $S\left(\sigma_M, \lambda\right)$ or $S\left(\sigma_M(t), \lambda(t)\right)$ when the dependence on σ_M and λ needs to be emphasized. Otherwise, we denote as S for brevity. In the next subsection, a sliding mode-based guidance law that stabilizes S at the origin is designed based on the Lyapunov stability theory. The condition in (2.4c) is also taken into account during the design process in order to satisfy the FOV constraint.

2.2.2 Derivation of guidance law

From (2.1) and (2.3), the dynamics of S in (2.7) is obtained as

$$\dot{S} = \frac{a_M}{V_M} + \Delta \tag{2.12}$$

where the unknown term Δ composed of the LOS rate is

$$\Delta = -\left[1 + k_1 \frac{\partial}{\partial e_1} \left\{\text{sgmf}(e_1, \phi_1)\right\}\right] \dot{\lambda} \tag{2.13}$$

and its magnitude is bounded as

$$\begin{aligned} |\Delta| \leq & \frac{V_M}{R_f} \left\{1 + k_1 \frac{\phi_1^2}{\left(e_1^2 + \phi_1^2\right)^{3/2}}\right\} |\sin \sigma_M| \\ \triangleq & \frac{V_M}{R_f} f_2(\sigma_M, \lambda) \end{aligned} \tag{2.14}$$

The term $f_2(\sigma_M, \lambda)$ represents

$$f_2(\sigma_M, \lambda) = \left\{1 + k_1 \frac{\phi_1^2}{\left(e_1^2 + \phi_1^2\right)^{3/2}}\right\} |\sin \sigma_M|. \tag{2.15}$$

Based on the dynamics in (2.12), I propose a sliding mode guidance law for the convergence of S as follows:

$$a_M = -\left\{\frac{V_M}{R_f} f_2\left(\sigma_M, \lambda\right) + k_2\right\} V_M \text{sgn}\left(S\right) \tag{2.16}$$

where k_2 is a positive constant and $\text{sgn}(\cdot)$ represents the signum function. In this work, the finite time convergence of S is required since the desired conditions (2.5) and (2.6) should be achieved before the interception to fulfill the impact angle control. Therefore, sliding mode control is appropriate for designing the guidance law owing to its capability to allow finite time convergence.

Note that the proposed command in (2.16) does not include any variable of the LOS rate or range because S and $f_2(\sigma_M, \lambda)$ in (2.16) are composed of only the look angle and LOS angle as shown in (2.7) and (2.15). Therefore, just bearings-only measurement is enough for the implementation of the proposed guidance law.

Now, the closed-loop dynamics of S is obtained by substituting (2.16) into (2.12) as follows:

$$\dot{S} = -\left\{\frac{V_M}{R_f} f_2\left(\sigma_M, \lambda\right) + k_2\right\} \operatorname{sgn}(S) + \Delta. \tag{2.17}$$

Since achieving the sliding mode $S = 0$ enables the interception of the stationary target at the designated impact angle as shown in subsection 2.2-A, the stability of $S = 0$ is verified using the closed-loop dynamics of (2.17) in next section 2.3.

2.3 Analysis of the proposed law

This section substantiates that the proposed guidance law satisfies the desired constraints through three subsections. In subsection 2.3-A, it is confirmed that the look angle does not violate the prescribed FOV constraint under the proposed law. In subsection 2.3-B, the stability of S at the origin is analyzed based on the closed-loop dynamics to verify the performance of the proposed law. Subsection 2.3-C examines the finite time convergence of e_1 and e_2 to investigate whether the proposed law achieves the kinematic conditions for the impact angle control before the interception.

2.3.1 Look angle analysis

To check whether the proposed law satisfies the FOV constraint, let us analyze the dynamics of the look angle σ_M under the proposed law as follows:

Theorem 2.1. *Consider the guidance law in (2.7) and (2.16) with the parameter k_1 satisfying (2.10). Then, for all initial conditions satisfying $|\sigma_M(0)| \leq \sigma_M^{\max}$, the look angle is*

always bounded as

$$|\sigma_M(t)| \leq \sigma_M^{\max} \quad \forall t \geq 0. \tag{2.18}$$

Proof. Consider a compact set $\mathbb{A} \triangleq \{\sigma_M : |\sigma_M| \leq \sigma_M^{\max}\}$ for the proof. Now, on $\sigma_M = \sigma_M^{\max}$, the time derivative of σ_M is rewritten as

$$\begin{aligned}\dot{\sigma}_M\Big|_{\sigma_M=\sigma_M^{\max}} =& \frac{a_M}{V_M} - \dot{\lambda}\Big|_{\sigma_M=\sigma_M^{\max}} \\ =& -\left\{\frac{V_M}{R_f} f_2(\sigma_M^{\max}, \lambda) + k_2\right\} \operatorname{sgn}\Big(S\left(\sigma_M^{\max}, \lambda\right)\Big) + \frac{V_M \sin \sigma_M^{\max}}{R}\end{aligned} \tag{2.19}$$

In (2.19), $S(\sigma_M^{\max}, \lambda)$ is always positive because k_1 is chosen as (2.10). Furthermore, from (2.15), the term $f_2(\sigma_M^{\max}, \lambda)$ in (2.19) is bounded from below as

$$f_2(\sigma_M^{\max}, \lambda) > \sin \sigma_M^{\max}. \tag{2.20}$$

Substituting (2.20) into (2.19) yields

$$\dot{\sigma}_M\Big|_{\sigma_M=\sigma_M^{\max}} < -\left(\frac{V_M}{R_f} \sin \sigma_M^{\max} + k_2\right) + \frac{V_M \sin \sigma_M^{\max}}{R} \tag{2.21}$$

Applying $R \geq R_f$ to inequality in (2.21) leads to

$$\dot{\sigma}_M\Big|_{\sigma_M=\sigma_M^{\max}} < -k_2 \tag{2.22}$$

Likewise, on $\sigma_M = -\sigma_M^{\max}$, the following is also satisfied:

$$\dot{\sigma}_M\Big|_{\sigma_M=-\sigma_M^{\max}} > k_2 \tag{2.23}$$

Consequently, the proposed law makes the set $|\sigma_M(t)| \leq \sigma_M^{\max}$ invariant, which proves (2.18). □

Theorem 2.1 verifies that the proposed guidance law in (2.16) achieves $|\sigma_M(t)| \leq \sigma_M^{\max}$ if the initial condition satisfies $|\sigma_M(0)| \leq \sigma_M^{\max}$. That is, the proposed law keeps the missile look angle within the prespecified FOV limit until the interception.

2.3.2 Stability analysis

In order to verify the performance of the proposed law, this subsection investigates the stability of the surface variable S in (2.7). For the investigation, the closed-loop dynamics in (2.17) is analyzed as follows:

Theorem 2.2. *Consider the dynamics of the surface variable (2.17). Then, the surface variable $S(t)$ reaches zero in a finite time t_r that is bounded as*

$$t_r \leq \frac{|S\left(\sigma_M(0), \lambda(0)\right)|}{k_2} \tag{2.24}$$

Proof. For the proof, consider the Lyapunov candidate function as

$$V = \frac{1}{2}S^2. \tag{2.25}$$

From (2.17), the time derivative of V is obtained as

$$\dot{V} = S\left[-\left\{\frac{V_M}{R_f}f_2(\sigma_M, \lambda) + k_2\right\}\operatorname{sgn}(S) + \Delta\right] \tag{2.26}$$

Using (2.14) into (2.26) gives

$$\begin{aligned}\dot{V} \leq & -\left\{\frac{V_M}{R_f}f_2(\sigma_M, \lambda) + k_2\right\}|S| + \frac{V_M}{R_f}f_2(\sigma_M, \lambda)|S| \\ = & -k_2\sqrt{2V}\end{aligned} \tag{2.27}$$

which implies that S is bounded and origin of the closed-loop dynamics in (2.17) is asymp-

totically stable. Furthermore, from [43], integrating the inequality (2.27) over $[0, t]$ yields

$$V^{1/2}(t) \leq -\frac{1}{\sqrt{2}} k_2 t + V^{1/2}(0), \tag{2.28}$$

which implies that $V(t)$ goes to zero in a finite time t_r bounded as

$$t_r \leq \frac{\sqrt{2} V^{1/2}(0)}{k_2} = \frac{|S\left(\sigma_M(0), \lambda(0)\right)|}{k_2}. \tag{2.29}$$

□

Theorem 2.2 shows that the sliding mode $S = 0$ is achieved in a finite time. From (2.7) and (2.11), hence, the proposed guidance law in (2.16) makes the errors e_1 and e_2 approach zero. However, for achieving the homing and impact angle conditions in (2.5) and (2.6) conclusively, e_1 and e_2 have to go to zero *before* the interception. Thus, in the next subsection, the finite time convergence of e_1 and e_2 is analyzed to prove the validity of the proposed guidance law.

2.3.3 Convergence analysis of error variables e_1 and e_2

From Theorem 2.2 in section 2.3-B, it is deduced that the convergence speed of S can be made faster by increasing the user-chosen parameter k_2. Furthermore, as shown in (2.11), it has already been proven that e_1 and e_2 converge to zero after $S = 0$ is achieved. However, unlike S whose convergence speed can be made arbitrarily faster, the convergence speed of e_1 is limited since the magnitude of the parameter k_1, related to the convergence of e_1, is restricted as shown in (2.10). Thus, it is necessary to verify that e_1 and e_2 go to zero before the end of the homing in order to guarantee the success of the desired tasks.

This subsection investigates the dynamics of e_1 to prove the finite time convergence of e_1 and e_2 under $S = 0$. For the convergence analysis, the following lemma is obtained priorly.

Lemma 2.1. *Let $f : [-1, 1] \to \mathbb{R}$ be a function such that*

$$f(x) = \sin(kx) \tag{2.30}$$

where the constant k is chosen as $0 < k \leq \frac{\pi}{2}$. Then, the function f satisfies

$$\begin{cases} f(x) \geq xf(1) & \text{if } x \in [0, 1] \quad (2.31a) \\ f(x) \leq xf(1) & \text{if } x \in [-1, 0] \quad (2.31b) \end{cases}$$

Proof. Let us prove the case $f(x) \geq xf(1)$ because the other case can be proved by the same way. In the domain $x \in [0, 1]$, f is a concave function since the second derivative of f is given by

$$\frac{d^2 f}{dx^2}(x) = -k^2 \sin(kx) \leq 0. \tag{2.32}$$

Therefore, from the definition of the concave function, it is satisfied that

$$f\left((1-t)x_1 + tx_2\right) \geq (1-t)f(x_1) + tf(x_2) \tag{2.33}$$

for any x_1, x_2 and $t \in [0, 1]$. Substituting 0 and 1 into x_1 and x_2 in (2.33) respectively yields

$$f(t) \geq tf(1), \tag{2.34}$$

which accords with the inequality property in (2.31a). □

Now, for the convergence analysis of e_1 and e_2, the following Theorem 2.3 is presented.

Theorem 2.3. *After the sliding mode $S = 0$ is achieved, the variables e_1 and e_2 in (2.8a) and (2.8b) converge to zero as the distance between the missile and target R goes to zero.*

Proof. For the proof, the following Lyapunov candidate function is introduced:

$$V_1 = \frac{1}{2}e_1^2. \tag{2.35}$$

First, let us prove the boundedness of e_1. On $S = 0$, the time derivative of V_1 is given by

$$\begin{aligned}
\dot{V}_1\Big|_{S=0} &= -\frac{V_M \sin\sigma_M}{R} e_1\Big|_{S=0} \\
&= -\frac{V_M}{R}\sin\left\{k_1 \mathrm{sgmf}(e_1, \phi_1)\right\} e_1 \\
&= -\frac{V_M}{R}\sin\left\{k_1 \frac{e_1}{\sqrt{e_1^2 + \phi_1^2}}\right\} e_1 \\
&\leq 0.
\end{aligned} \tag{2.36}$$

where the condition of k_1 in (2.10) is used. The result in (2.36) signifies that e_1 is bounded after S converges, so there exists a positive constant $e_1^{\max}$ such that $|e_1(t)|_{S=0} \leq e_1^{\max}$. Then, from (2.36), it is obtained that

$$\dot{V}_1\Big|_{S=0} \leq -\frac{V_M}{R}\sin\left\{k_1 \frac{e_1}{\sqrt{(e_1^{\max})^2 + \phi_1^2}}\right\} e_1. \tag{2.37}$$

In (2.37), the relative range R satisfies $R \leq V_M t_{go} = V_M(t_f - t)$ where t_{go} and t_f denote the remaining time-to-go and impact time of the missile respectively, since R is the shortest distance between the missile and target. Furthermore, by Lemma 2.1, the sine term in (2.37) satisfies

$$\begin{cases}
\sin\left\{k_1 \dfrac{e_1}{\sqrt{(e_1^{\max})^2 + \phi_1^2}}\right\} \geq (\sin k_1)\dfrac{e_1}{\sqrt{(e_1^{\max})^2 + \phi_1^2}} & \text{if } e_1 \geq 0 \qquad (2.38\text{a}) \\
\sin\left\{k_1 \dfrac{e_1}{\sqrt{(e_1^{\max})^2 + \phi_1^2}}\right\} \leq (\sin k_1)\dfrac{e_1}{\sqrt{(e_1^{\max})^2 + \phi_1^2}} & \text{if } e_1 \leq 0 \qquad (2.38\text{b})
\end{cases}$$

Accordingly, using these properties yields

$$\begin{aligned}\dot{V}_1\Big|_{S=0} &\leq -\frac{\sin k_1}{t_{go}}\frac{e_1^2}{\sqrt{(e_1^{\max})^2+\phi_1^2}} \\ &\leq -\frac{2\sin k_1}{\sqrt{(e_1^{\max})^2+\phi_1^2}}\frac{V_1}{t_{go}},\end{aligned} \tag{2.39}$$

which implies

$$V_1(t)\Big|_{S=0} \leq V_1(0)\left(\frac{t_{go}}{t_f}\right)^{\frac{2\sin k_1}{\sqrt{(e_1^{\max})^2+\phi_1^2}}}. \tag{2.40}$$

The inequality in (2.40) implies that $V_1(t)$ goes to zero as t approaches t_f, which also yields $\lim_{t\to t_f} e_2 = 0$ because $e_2 = k_1\mathrm{sgmf}(e_1, \phi_1)$ on $S = 0$. Therefore, if the regulation of S is achieved, both e_1 and e_2 converge to zero as the missile approaches the stationary target. □

Theorem 2.2 implies that the sliding mode can be achieved before the end of the homing by adjusting the gain k_2. Theorem 2.3 indicates that achievement of the sliding mode makes e_1 and e_2 converge to zero before the end of the homing since the homing is terminated when the relative R goes to zero. Consequently, the error variables e_1 and e_2 can be made zero before the end of the homing, which verifies that the proposed guidance law in (2.16) can satisfy the kinematic conditions in (2.5) and (2.6) during the homing. That is, the interception with the desired impact angle can be achieved under the proposed law.

From Theorem 2.3, it is verified that the proposed guidance law in (2.16) satisfies the kinematic conditions in (2.5) and (2.6) during the homing. That is, the interception with the desired impact angle can be achieved under the proposed law.

2.4 Simulation results

This section evaluates the performance of the proposed guidance law by carrying out numerical simulations. In subsection 2.4-A, the validity of the proposed guidance law for various

terminal impact angles and field-of-view (FOV) constraints is demonstrated. In subsection 2.4-B, the proposed guidance law is compared with other FOV-constrained impact angle control guidance laws. In subsection 2.4-C, the performance of the proposed law in practical applications is examined using a realistic interceptor model.

When the proposed law is applied, to avoid the chattering caused by the discontinuity, the signum function $\mathrm{sgn}(\cdot)$ in (2.16) is approximated as the following continuous hyperbolic tangent function [9, 10, 27]:

$$\tanh(ax) = 2\left(\frac{1}{1+\exp^{-2ax}} - \frac{1}{2}\right) \tag{2.41}$$

Applying such an approximation makes the variable converge to the ideal sliding mode with slight deviation which is approximately in inverse proportion to a [44]. The value of a as $a = 10$ is used in this paper.

In addition, the acceleration command of the missile is saturated within $\pm 10g$, and the homing is terminated when the relative range R is less than or equal to 0.5 m in all the scenarios. The parameters used in the proposed guidance law are listed in Table 2.1.

Table 2.1: Simulation setting

Parameters	Values
Initial position of the missile $(x_M(0), y_M(0))$	$(0, 0)$ km
Position of the stationary target $(x_T(0), y_T(0))$	$(10, 0)$ km
Initial missile look angle $\sigma_M(0)$	15 deg
Missile speed V_M	250 m/s
Missile acceleration limits $\lvert a_M \rvert^{\max}$	10 $g^{\dagger}$
Guidance gains	$k_1 = \sigma_M^{\max} - 0.01,\ k_2 = 10,\ R_f = 0.5$ $\phi_1 = 0.15,\ \phi_2(0) = 0.002,\ k_\phi = 0.01$

† g means the gravitational acceleration, i.e., $g = 9.81$ m/s^2.

2.4.1 Performance analysis of the proposed law

For the simulations of the performance analysis, this subsection considers two scenarios. The first scenario deals with engagements for different impact angle constraints with a fixed look angle limitation of $\sigma_M^{\max} = 45°$. The second scenario considers engagements for a fixed impact angle constraint of $\gamma_d = -60°$ with various look angle limitations.

The results of the first scenario are presented as Figs. 2.2a∼d. In the figures, the results for the desired impact angles of $-30°$, $-60°$, $-90°$ and $-120°$ are represented by the triangular, inverted triangular, rectangular and circular patterned-lines respectively.

Under the proposed guidance law, the missile intercepts the target for all the cases as illustrated by Fig. 2.2a. Specifically, figure 2.2b shows that the proposed law achieves the sliding mode with the lateral acceleration not exceeding $\pm 10g$. Owing to using the hyperbolic tangent function in (2.41) instead of the discontinuous signum function in the guidance command, it is seen that the convergence of S is obtained without undesirable high-frequency chattering. Since the sliding mode is achieved, both the errors e_1 and e_2 also approach zero as shown in Fig. 2.2c. In particular, it is observed that e_1 and e_2 converge to zero before the interception as proven by Theorem 2.3 in section 2.3-C. Accordingly, the upper row of figure 2.2d provides the result that the proposed law achieves the desired impact angle for all the cases.

The trajectories in figure 2.2a also show that the missile takes a longer bypass as the higher impact angle is demanded. Nevertheless, the lower row of figure 2.2d shows that the look angle does not violate the prescribed limit $\sigma_M^{\max} = 45°$ for all the cases under the proposed guidance law. This result accords with Theorem 2.1 in section 2.3-A.

Figures 2.3a∼d provide the simulation results of the second scenario. Likewise, the results with the look angle limits of 15°, 30°, 45° and 60° are denoted as the triangle, inverted triangle, square and circle patterned-lines respectively in each figure.

Figure 2.3a demonstrates that the proposed law achieves the interception under all the considered FOV limits. Like the first scenario, the surface variable converges near zero

at the initial stage, and then the error variables e_1 and e_2 also approach zero before the interception as shown in Figs 2.3b and 2.3c. As a result, it is observed by the upper row of Fig. 2.3d that the desired impact angles can be achieved for all the cases.

Figure 2.3a also shows that the curvatures are different from one another although the terminal impact angle is same in all the four cases. It is because all the four missiles fly under the differently prescribed values of the look angle constraints as given in the lower graph of Fig. 2.3d. This result demonstrates that the proposed guidance law can restrict the maximum look angle as desired, as proven in Theorem 2.1.

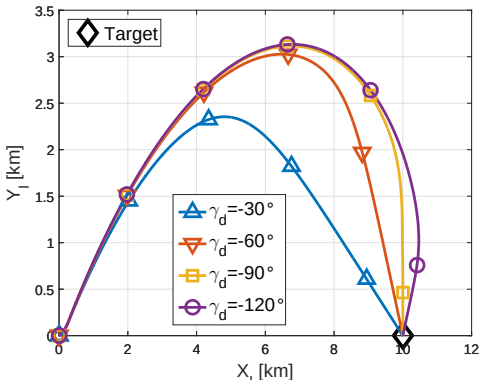

(a) Flight trajectories with $\sigma_M^{\max} = 45°$

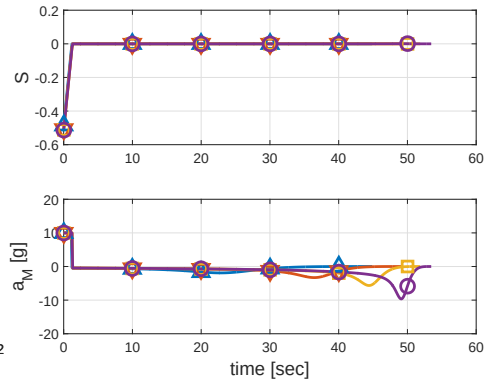

(b) Surface variables S and guidance commands with $\sigma_M^{\max} = 45°$

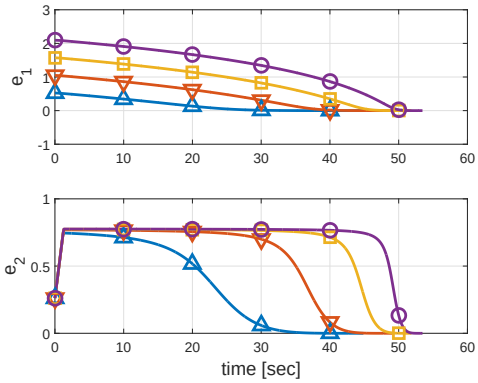

(c) Error variables e_1 and e_2 with $\sigma_M^{\max} =$ 45°

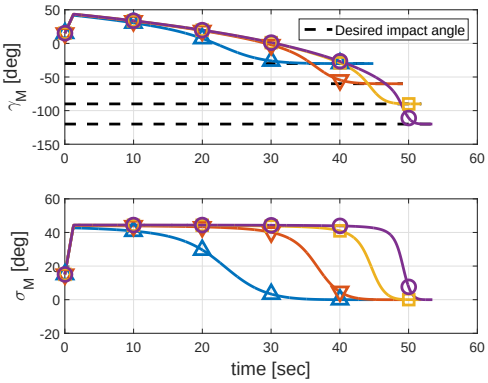

(d) Flight path angles and look angles with $\sigma_M^{\max} = 45°$

Figure 2.2: Simulation results for different impact angle constraints with a fixed look angle limitation of $\sigma_M^{\max} = 45°$

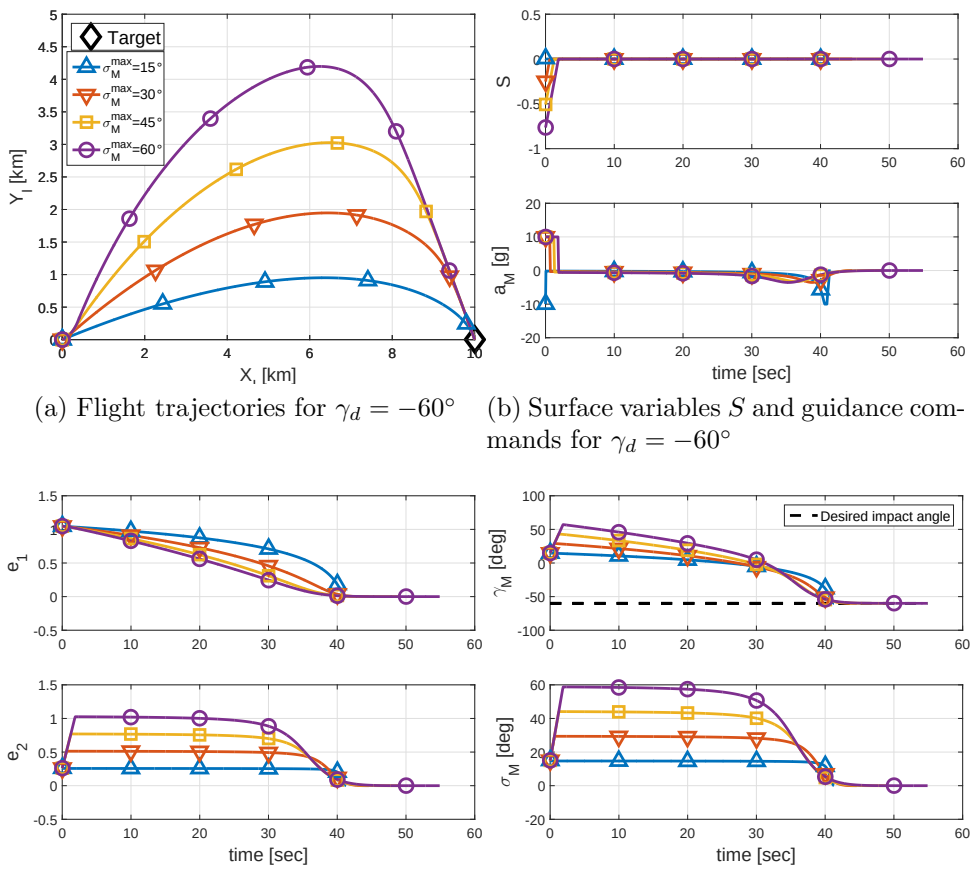

(a) Flight trajectories for $\gamma_d = -60°$

(b) Surface variables S and guidance commands for $\gamma_d = -60°$

(c) Error variables e_1 and e_2 for $\gamma_d = -60°$

(d) Flight path angles and look angles for $\gamma_d = -60°$

Figure 2.3: Simulation results for a fixed impact angle constraint of $\gamma_d = -60°$ with various look angle limitations

2.4.2 Performance comparison with other guidance laws

In this subsection, the proposed law is compared with other impact angle control guidance laws that consider the FOV limit called ROG (range-to-go weighted optimal guidance law) and TPPN (two-stage pure proportional navigation guidance law) developed in [15] and [20] respectively. ROG and TPPN are linear and nonlinear dynamics-based laws respectively, and both of them are the most recently developed laws among related research at the time of this study. These laws are generated as the following forms:

ROG [15] : (2.42)

$$a_M = \begin{cases} -(N+3)V_M^2\left(\frac{\sigma_M R-\sigma_M^{\max}R_1}{R^{N+3}-R_1^{N+3}}\right)R^{N+1}+\mu\frac{R^N}{V_M^2}\left\{1-\left(\frac{N+3}{N+2}\right)\left(\frac{R^{N+2}-R_1^{N+2}}{R^{N+3}-R_1^{N+3}}\right)\right\} & \text{for } R_1 < R \le R_0 \\ V_M\dot{\lambda} & \text{for } R_2 < R \le R_1 \\ -\frac{V_M^2}{R}\left\{(N+2)(N+3)\sigma_M+(N+1)(N+2)(\gamma_d-\gamma_M)\right\} & \text{for } R_f < R \le R_2 \end{cases}$$

TPPN [20] : (2.43)

$$a_M = \begin{cases} V_M\dot{\lambda} \\ N_s V_M\dot{\lambda} \end{cases} \quad \text{switches at } \lambda = \gamma_d + \frac{\sigma_M(0)}{(N_s-1)}$$

In (2.42) and (2.43), we set the parameters N and N_s as $N = 1$ and $N_s = 3$ respectively. Both settings ensure satisfaction of the impact angle and look angle constraints, and are also used in [15] and [20] respectively. Values of the other parameters such as μ, R_1 and R_2 in (2.42) are determined by initial conditions and the value of N.

As a simulation setting for the performance comparison, the desired impact angle is fixed as $\gamma_d = -60°$ and the FOV limit of $\sigma_M^{\max} = 30°$ is applied for all three guidance laws. The initial conditions in Table 2.1 are also considered for the guidance laws except that the initial look angle for TPPN is set to be 30° instead of 15°. It is because TPPN is designed so that it tries not to exceed the FOV limit by maintaining the initial look angle during the first phase as explained in detail in [20]. That is, the engagement conditions in this subsection are set to make the look angles under all the laws are constrained by the same

limit, i.e. $\sigma_M^{\max} = 30°$, for fair comparison.

Figures 2.4a∼d give the results for an impact angle constraint of $\gamma_d = -60°$ with a look angle limitation of $\sigma_M^{\max} = 30°$ under three different guidance laws. The results under ROG, TPPN and the proposed law are denoted as the triangle, inverted triangle and circle-patterned line respectively.

Figure 2.4a shows that all the three guidance laws intercept the stationary target with similar trajectories. The terminal constraints on the terminal impact angle of $\gamma_d = -60°$ are also achieved without violating the look angle limit of $\sigma_M^{\max} = 30°$ under all the laws as presented by Figs. 2.4b and 2.4c.

Figure 2.4d provides the guidance commands under three laws. At the initial stage of the homing, TPPN generates a smaller guidance command compared with the other laws because it does not need to change the look angle as shown in Fig. 2.4c. This property of TPPN to maintain its initial look angle prevents the command from saturating at the initial stage. However, to achieve this property requires that the missile be launched at a deviated look angle from the target. Furthermore, since TPPN switches the navigation constant for achieving the desired impact angle, there must be an undesirable discontinuity in the guidance command as shown in Fig. 2.4d.

Unlike TPPN, both ROG and the proposed guidance law generate continuous commands. In particular, ROG produces the acceleration command of more modest amplitude than the other two laws except for at the initial stage, which results from its optimality property as described in detail in [15]. However, as shown in (2.42), the implementation of ROG needs values of transition points R_1 and R_2, which requires a numerical computation process. Hence, not enough iterations caused by lack of calculation time or capacity can result in performance degradation when employing ROG. Moreover, as shown in (2.16), (2.42) and (2.43), ROG necessitates the information of the relative range R while TPPN and the proposed law does not. That is, measurement or estimation of R is required for the implementation of ROG unlike TPPN and the proposed law.

In contrast, the result in Figs. 2.4a∼c shows that the proposed law can fulfill the impact

angle control without violating the prescribed look angle limit although its implementation does not require the information of LOS rate and relative range. Figure 2.4d shows that the proposed law produces a large command at the initial stage to make S converge to zero, but the generated command is continuous and not large after the initial stage. That is, the practical application of the proposed law is more helpful to restricted guidance scenarios where only bearing angles are measurable in comparison with other existing laws.

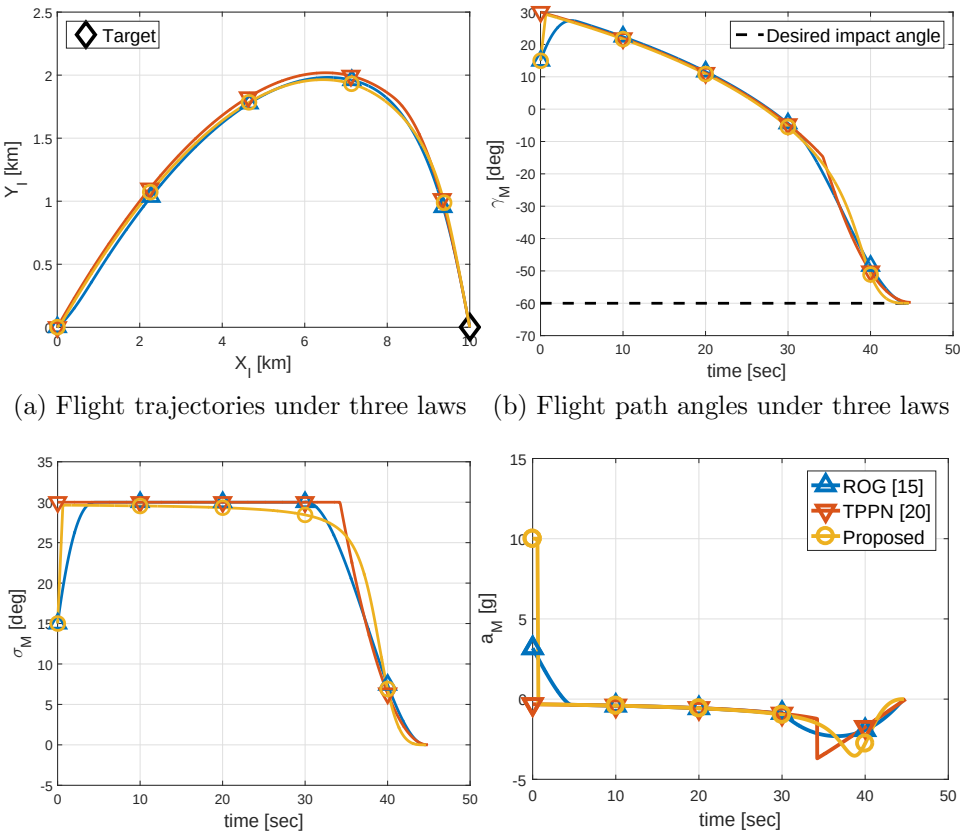

(a) Flight trajectories under three laws (b) Flight path angles under three laws

(c) Look angles under three laws (d) Guidance commands under three laws

Figure 2.4: Simulation results under three different guidance laws: ROG, TPPN and the proposed law

2.4.3 Performance analysis in a realistic scenario

This subsection carries out engagement simulations considering rotational dynamics of the missile to evaluate the performance of the proposed law in realistic applications. Involving the aerodynamics and gravitation, the lateral maneuvering acceleration is produced by the aerodynamic lift as

$$a_M = \frac{L(\alpha, \delta)}{m} \tag{2.44}$$

and the angle-of-attack α is governed by the rotational motion as

$$\begin{aligned} \dot{\alpha} =& q - \frac{L(\alpha, \delta) - mg\cos\gamma_M}{mV_M}, \quad \dot{\theta} = q \\ \dot{q} =& \frac{M(\alpha, q, \delta)}{I_{yy}}, \quad \dot{\delta} = \frac{\delta_C - \delta}{\tau_\delta}. \end{aligned} \tag{2.45}$$

θ, q, δ and δ_C represent the pitch angle, pitch rate, canard deflection and command of the canard deflection respectively. $L(\cdot)$ and $M(\cdot)$ mean the lift force and pitching moment, and m, I_{yy} and τ_δ denote the mass, moment of inertial with respect to the pitch axis and time constant of the canard dynamics. The detailed aerodynamic model for the lift force and pitch moment in (2.45) is described in [45] and [9].

Based on the realistic model, the same scenario in Fig. 2.2 is applied, so the desired impact angles of $-30°$, $-60°$, $-90°$ and $-120°$ with the fixed look angle limitation of $45°$ are considered. Since the angle-of-attack is not neglected in this realistic scenario, the look angle defined as the angle between the LOS and missile heading is re-expressed as

$$\begin{aligned} \sigma_M^{act} =& \theta - \lambda \\ =& \sigma_M + \alpha. \end{aligned} \tag{2.46}$$

In order not to violate the FOV limit, the restriction of the actual look angle in (2.46) is required as $|\sigma_M^{act}| \leq 45°$. To achieve the actual restriction for σ_M^{act}, σ_M in the guidance

command (2.16) is restricted with a safety margin ε_σ, i.e., $|\sigma_M| \leq 45^\circ - \varepsilon_\sigma$. From (2.46), it is reasonable that the maximum value of the angle-of-attack is selected as the safety margin. In general missile configurations, the angle-of-attack is approximately proportional to the lateral acceleration caused by the lift force as

$$\alpha \approx \frac{m}{QS_{ref}C_{L_\alpha}} a_M \tag{2.47}$$

where m, Q, S_{ref}, and C_{L_α} denote the mass, dynamic pressure, reference area, and coefficient of lift to angle-of-attack. Substituting $a_M = a_M^{\max} = 10\,g$ into (2.47) yields the maximum angle-of-attack, and it is calculated as $\alpha_{\max} = 4.425^\circ$ in this case. Accordingly, we choose the safety margin as $\varepsilon_\sigma = 4.5^\circ$ for this simulation in this subsection. In addition, to compensate the gravitational effect in vertical plane, the term $g\cos\gamma_M$ is added to the original command in (2.16).

Figure 2.5 presents the simulation results for the realistic scenario. The results for the desired impact angles of $\gamma_d = -30^\circ$, -60°, -90° and -120° are denoted as the triangle, inverted triangle, square and circle patterned-lines respectively. As shown in Figs. 2.5a and 2.5b, the missile intercepts the stationary target at the desired impact angle for all cases.

From Figs. 2.5c and 2.5d, it is confirmed that the proposed law satisfies the look angle limit of $\sigma_M^{act} = 45^\circ$ with feasible lateral accelerations for all the desired impact angles. Figure 2.5c also shows that the actual look angle defined as (2.46) reaches its peak momentarily at the initial stage of the homing for every case. This large demand on the actual look angle is caused by the fact that the large requirement on the lateral acceleration at the initial stage shown in (2.5d) induces the large angle-of-attack. Nevertheless, the actual look angle does not violate the prescribed limit since the proposed law restricts the ideal look angle σ_M with the safety margin ε_σ as described above.

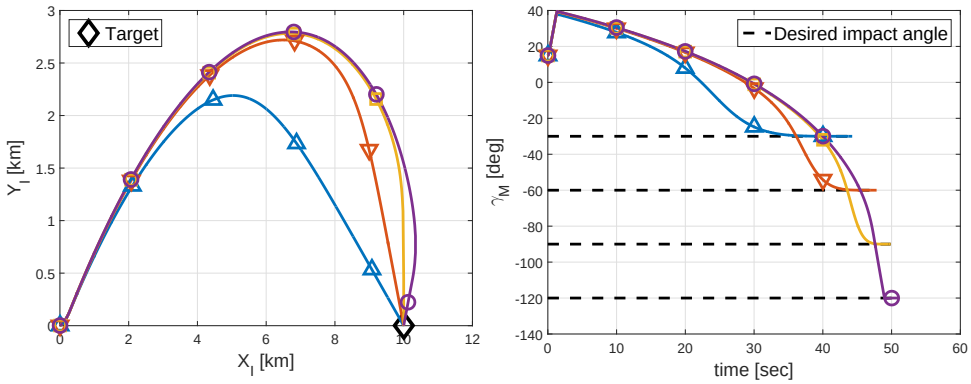

(a) Flight trajectories in a realistic scenario

(b) Flight path angles in a realistic scenario

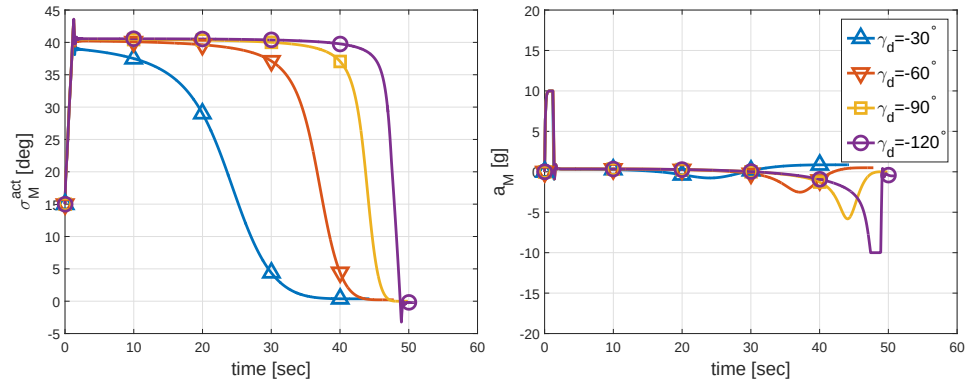

(c) Actual look angles in a realistic scenario

(d) Lateral accelerations in a realistic scenario

Figure 2.5: Simulation results in a realistic scenario

3

Impact Time Control Guidance with Field-of-View Constraint

This chapter proposes a guidance law that achieves the desired terminal impact time without violating a seeker's field-of-view (FOV) limit. In order to derive the guidance law, kinematic conditions for impact time control are defined, and the backstepping control technique is applied for the satisfaction of the conditions. As a virtual control input for the backstepping structure, the missile look angle, which represents the angle between the line-of-sight and missile heading vector, is used and its magnitude is limited by a prescribed limit. Then, the seeker's look angle can also be confined within a specific range because the seeker look angle is mainly determined by the difference between the line-of-sight (LOS) and the heading vector. This capability to confine the seeker's look angle with achieving the desired impact time is the main contribution of the paper. To evaluate the performance of the proposed law, numerical simulations are conducted for various engagement scenarios. The contents of this chapter are also available in the open literature of [47].

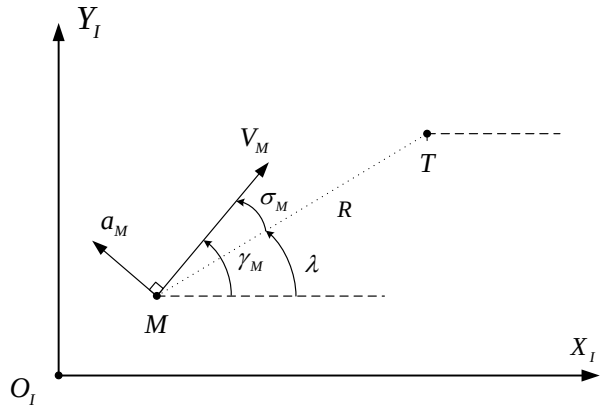

Figure 3.1: Two-dimensional engagement geometry for a stationary target

3.1 PROBLEM FORMULATION

This section presents the dynamics of the missile-target engagement in order to formulate the guidance problem about impact time control. As shown in Fig. 3.1, let us consider a two-dimensional engagement geometry in the inertial coordinate frame $X_I O_I Y_I$. In the Fig. 3.1, R and λ denote the relative range and LOS (line-of-sight) angle between the missile and target which are represented by the points M and T respectively. Also, V_M, a_M, γ_M and σ_M denote the speed, normal acceleration, flight path angle and look angle of the missile, respectively. Then, the governing equations of the engagement dynamics are expressed in terms of R and λ as follows:

$$\dot{R} = V_R \tag{3.1a}$$

$$R\dot{\lambda} = V_\lambda \tag{3.1b}$$

where V_R and V_λ are relative velocity components of the target with respect to the missile along and normal to the LOS respectively, and can be expressed as

$$V_R = -V_M \cos\sigma_M \tag{3.2a}$$

$$V_\lambda = -V_M \sin\sigma_M. \tag{3.2b}$$

It is assumed that the maneuvering acceleration of the missile is applied normal to the velocity vector, so the equation about the flight path angle is given by

$$\dot{\gamma}_M = \frac{a_M}{V_M}. \tag{3.3}$$

In this problem, the missile acceleration a_M is used as the control input of the guidance problem. Therefore, to develop the guidance command a_M that enables the missile to intercept the target at the desired impact time is the design objective in this study.

3.2 IMPACT TIME CONTROL GUIDANCE LAW WITH CONSTRAINED FIELD-OF-VIEW LIMITS

In this section, the suitable kinematic conditions for satisfying the desired terminal constraints are established, and the impact time control guidance law is designed based on the proposed conditions.

3.2.1 Kinematic conditions for impact time control guidance

This subsection includes the kinematic conditions that allow the missile to intercept the target at the desired impact time without needing to perform the time-to-go estimation. Furthermore, the field-of-view limitation of the missile's seeker is considered by setting bounds to the look angle.

A basic concept for the interception to a stationary target is to make the missile move toward the target along the LOS, which can be expressed mathematically as

$$V_\lambda = 0 \tag{3.4a}$$

$$V_R < 0. \tag{3.4b}$$

The homing conditions in (3.4) can be converted into a single condition:

$$\sigma_M = 0. \tag{3.5}$$

That is, satisfying the condition in (3.5) guarantees the missile to be on the collision path against the target.

The impact time constraint is achieved if the actual remaining time-to-go t_{go} is equal to the desired time-to-go t_{go}^d, which is expressed as

$$t_{go} = t_{go}^d \tag{3.6}$$

where the desired time-to-go t_{go}^d is defined as $t_{go}^d = t_d - t$. Unlike t_{go}^d whose value is explicitly determined, the actual time-to-go t_{go} is difficult to be calculated accurately under general engagement situations. However, on the collision path satisfying (3.5), the time-to-go is certainly determined as

$$t_{go}\Big|_{\sigma_M=0} = \frac{R}{V_M} \tag{3.7}$$

since the missile flies straight to the target. Then, from (3.6) and (3.7), a condition for satisfying the desired impact time on the collision path can be formulated as

$$\begin{aligned} R =& R_d \\ \triangleq& V_M t_{go}^d. \end{aligned} \tag{3.8}$$

That is, if the missile on the collision path approaches the target with satisfying (3.8), the impact time constraint in (3.6) is achieved. Therefore, satisfaction of both conditions in (3.5) and (3.8) guarantees the interception of the target at the desired impact time.

To consider the FOV limits in the guidance problem, the look angle between the LOS and missile heading vector needs to be limited because it almost determines the seeker look

angle. Particularly when the angle-of-attack of the missile is small enough to be neglected, the seeker look angle becomes approximately equal to the look angle σ_M. Therefore, in order to handle the FOV limits, the limitation of the missile look angle is considered as follows:

$$|\sigma_M| \leq \sigma_M^{\max} \leq \pi/2 \tag{3.9}$$

where $\sigma_M^{\max}$ is the acceptable maximum value of the missile look angle. In this problem, it is assumed that the condition in (3.9) represents the FOV limits from neglecting the angle-of-attack dynamics.

As a result, fulfilling the proposed kinematic conditions in (3.5), (3.8) and (3.9) guarantees that the missile intercepts the target at the desired impact time without violating the FOV limits. In the next subsection 3.2.2, the guidance law is designed to satisfy these kinematic conditions.

3.2.2 Guidance law design

As explained in the previous subsection 3.2.1, the design objective for deriving the guidance law is the fulfillment of two equality conditions in (3.5) and (3.8) under keeping the inequality condition in (3.9). In order to satisfy the proposed kinematic conditions, error variables can be defined intuitively as

$$\begin{aligned} e_1 &= R^d - R \\ &= V_M t_{go}^d - R \qquad (3.10a) \\ e_2 &= \sigma_M. \qquad (3.10b) \end{aligned}$$

By regulating both the error variables in (3.10), the homing and impact time conditions in (3.5) and (3.8) respectively can be satisfied. The fulfillment of the inequality condition in (3.9) will be confirmed in section 3.3.

For the regulation of both variables, however, only the single command a_M is used as a control input, which implies that the system can be underactuated if the two error dynamics subject to the single control input are decoupled. To analyze this problem, let us take the time derivative of the error variables in (3.10) as follows:

$$\dot{e}_1 = -V_M + V_M \cos\sigma_M \tag{3.11a}$$

$$\dot{e}_2 = -\dot{\lambda} + \frac{a_M}{V_M}. \tag{3.11b}$$

where $\frac{d}{dt}\left(t_{go}^d\right) = -1$ is used to obtain (3.11a). It can be observed that the error dynamics in (3.11) are in strict-feedback form. Furthermore, the origin of (e_1, e_2) can be an equilibrium point because $e_2 = 0$ allows $\dot{e}_1 = 0$. Applying the backstepping control technique, accordingly, makes it possible to regulate both e_1 and e_2 by stabilizing e_1.

For the application of the backstepping control, let us define new error variables as

$$z_1 = V_M t_{go}^d - R \tag{3.12a}$$

$$z_2 = \sigma_M - \sigma_M^d \tag{3.12b}$$

where σ_M^d is the desired look angle that serves as a virtual control input for achieving the convergence of z_1. Taking the time derivative of the proposed error variables in (3.12) leads to

$$\dot{z}_1 = -V_M + V_M \cos\sigma_M \tag{3.13a}$$

$$\dot{z}_2 = -\dot{\lambda} - \dot{\sigma}_M^d + \frac{a_M}{V_M}. \tag{3.13b}$$

Based on the dynamics in (3.13), the virtual control input and guidance law for the stability

of z_1 and z_2 at the origin can be proposed as follows.

$$\sigma_M^d = \cos^{-1}\left(1 - k_1 \mathrm{sgmf}(z_1)\right) \tag{3.14a}$$

$$a_M = a_M^{eq} + a_M^{con} \tag{3.14b}$$

where

$$a_M^{eq} = V_M\left(\dot{\lambda} + \dot{\sigma}_M^d\right) \tag{3.15a}$$

$$a_M^{con} = -k_2 V_M \mathrm{sgn}(z_2), \tag{3.15b}$$

and the sigmoid function $\mathrm{sgmf}(\cdot)$ is chosen as

$$\mathrm{sgmf}(x) = \begin{cases} -\frac{1}{2\phi^3}x^3 + \frac{3}{2\phi}x & \text{if } |x| \leq \phi \\ \mathrm{sgn}(x) & \text{else} \end{cases}. \tag{3.16}$$

The controller gains k_1, k_2 and parameter ϕ are selected as positive constants. Here, it can be easily shown that the sigmoid function in (3.16) is continuously differentiable and has boundedness properties such that

$$|\mathrm{sgmf}(x)| \leq 1 \tag{3.17a}$$

$$\left|\frac{d}{dx}\left(\mathrm{sgmf}(x)\right)\right| \leq \frac{3}{2\phi}. \tag{3.17b}$$

These properties are used to analyze the guidance law in section 3.3. The signum function $\mathrm{sgn}(\cdot)$ in (3.15b) and (3.16) is defined as

$$\mathrm{sgn}(x) = \begin{cases} 1 & \text{if } x > 0 \\ 0 & \text{if } x = 0 \\ -1 & \text{if } x < 0 \end{cases} \tag{3.18}$$

In this problem, it is assumed that the relative range R, LOS angle λ, LOS rate $\dot{\lambda}$ and look angle σ_M are available by using a gimbal seeker and inertial navigation system (INS). Based on these measurements, the time derivative of the desired look angle $\dot{\sigma}_M^d$ in (3.15a) can be calculated as

$$\begin{aligned}\dot{\sigma}_M^d =& \frac{d}{dt}\left(\cos^{-1}\left(1 - k_1 \mathrm{sgmf}(z_1)\right)\right) \\ =& \frac{k_1}{\sin\sigma_M^d}\left(-V_M + V_M\cos\sigma_M\right)\frac{d}{dz_1}\mathrm{sgmf}(z_1) \\ =& \frac{k_1}{\sin\sigma_M^d}\left(-V_M + V_M\cos\sigma_M\right)\left(-\frac{3}{2\phi^3}z_1^2 + \frac{3}{2\phi}\right)\end{aligned} \tag{3.19}$$

which is a function of R and σ_M from the definitions of z_1 and σ_M^d in (3.12a) and (3.14a) respectively. Therefore, the guidance command proposed in (3.14) and (3.15) consists of measurable state variables.

Also, note that the desired look angle command in (3.14a) involves the arc cosine function $\cos^{-1}(\cdot)$ whose domain for yielding a real value is $[-1, 1]$. Hence, it is necessary to analyze whether its argument $(1 - k_1\mathrm{sgmf}(z_1))$ in (3.14a) belongs to $[-1, 1]$. The analysis is included in section 3.3.

Now, the closed-loop dynamics can be obtained by substituting (3.14) into (3.13):

$$\dot{z}_1 = -k_1 V_M \mathrm{sgmf}(z_1) + V_M \frac{\cos\sigma_M - \cos\sigma_M^d}{\sigma_M - \sigma_M^d} z_2 \tag{3.20a}$$

$$\dot{z}_2 = -k_2 \mathrm{sgn}(z_2). \tag{3.20b}$$

As explained earlier, the regulation of the variables z_1 and z_2 guarantees the interception of the target at the desired impact time. Accordingly, the stability of (z_1, z_2) at the origin is analyzed based on the closed-loop dynamics of (3.20) in section 3.3.

3.3 ANALYSIS OF THE PROPOSED GUIDANCE LAW

In this section, it is verified that the desired constraints are satisfied under the law. Prior to the performance analysis of the proposed law, the guidance command is investigated to examine the singularity problem in subsection 3.3.1. Based on the Lyapunov theory, the stability of the overall closed-loop dynamics is analyzed in subsection 3.3.2. To confirm whether the proposed law prevents the violation of the FOV limits, the look angle dynamics is also investigated in subsection 3.3.3. Besides, the achievable domain of the desired impact time under the proposed law is estimated in subsection 3.3.4 to be helpful in real applications.

3.3.1 Guidance command analysis

For the implementation of the law, the proposed guidance command should not include any non-computable term such as singular or imaginary. In this subsection, thus, a few suspected terms in the developed command are checked.

Since the desired look angle command σ_M^d in (3.14a) involves $\cos^{-1}(\cdot)$, the term $(1 - k_1 \mathrm{sgmf}(z_1))$ should be in $[-1, 1]$, which is satisfied by the following conditions:

$$0 \leq k_1 \leq 2 \tag{3.21}$$

$$0 \leq z_1(t). \tag{3.22}$$

Because the controller gain k_1 is chosen by the user, the condition in (3.21) can be achieved readily. Now, let us analyze the satisfaction of the condition in (3.22). Let $z_{1,f}$ be the maximum acceptable error of z_1, obtained by (3.12a) with the maximum allowable miss distance, and $t_{z_2=0}$ be the reaching time of $z_2(t)$ which means the minimum time achieving $z_2(t) = 0 \ \forall t \geq t_{z_2=0}$.

Theorem 3.1. *For all initial conditions satisfying $|z_1(0) - z_{1,f}| / (2V_M) > t_{z_2=0}$, the error variable $z_1(t)$ in (3.20) is always larger than or equal to zero, i.e., $z_1(t) \geq 0 \ \forall t \geq 0$.*

Proof. From (3.13a), the reaching time of $z_1(t)$, $t_{z_1=z_{1,f}}$ which means the minimum time achieving $|z_1(t)| \leq z_{1,f}$, has the following relationship.

$$t_{z_1=z_{1,f}} \geq \frac{|z_1(0) - z_{1,f}|}{\left|\max\limits_{\sigma_M} \dot{z}_1\right|} = \frac{|z_1(0) - z_{1,f}|}{2V_M} > t_{z_2=0}. \tag{3.23}$$

The result of (3.23) implies that $z_1(t) = 0$ does not occur before $z_2(t) = 0$, which also signifies that $z_1(t) = 0$ always involves $z_2(t) = 0$. Hence, the time derivative of z_1 when $z_1(t) = 0$ is obtained as

$$\dot{z}_1(t)\Big|_{z_1=0} = \dot{z}_1(t)\Big|_{z_1=0,z_2=0} = 0. \tag{3.24}$$

Therefore, $z_1(t)$ cannot decrease below zero, which means $z_1(t) \geq 0$ for all $t \geq 0$. □

From the closed-loop dynamics of $z_2(t)$ in (3.20b), the reaching time of $z_2(t)$, denoted as $t_{z_2=0}$ in Theorem 3.1, can be calculated as $t_{z_2=0} = |z_2(0)|/k_2$. The condition in (3.22), therefore, can be accomplished by satisfying the initial condition of

$$\frac{|z_1(0) - z_{1,f}|}{2V_M} > \frac{|z_2(0)|}{k_2}. \tag{3.25}$$

As a result, the arc cosine term can be implemented without any non-computability issue.

Besides, the equivalent component of the command in (3.15) contains the term $\dot{\sigma}_M^d$ expressed as

$$\dot{\sigma}_M^d = \frac{k_1 \dot{z}_1}{\sin \sigma_M^d} \frac{d}{dz_1} \mathrm{sgmf}(z_1), \tag{3.26}$$

which necessitates to check the possibility of $\sin \sigma_M^d = 0$. As it will be described later in section 3.3.3, the controller gain k_1 is chosen to satisfy

$$0 \leq k_1 < 1 - \cos \sigma_M^{\max}. \tag{3.27}$$

Thus, from the definition of σ_M^d in (3.14a), $\sin\sigma_M^d = 0$ implies $\sigma_M^d = 0$ which involves $z_1 = 0$. In Theorem 3.1, it has already been proven that $z_1(t) = 0$ involves $z_2(t)\left(= \sigma_M - \sigma_M^d\right) = 0$. Therefore, $\dot{\sigma}_M^d$ when $\sin\sigma_M^d = 0$ is calculated as

$$\lim_{\sin\sigma_M^d \to 0} \dot{\sigma}_M^d = \lim_{\sigma_M \to 0} \frac{k_1 V_M \left(\cos\sigma_M - 1\right)}{\sin\sigma_M} \frac{d}{dz_1}\mathrm{sgmf}(z_1) = 0, \tag{3.28}$$

which shows $\sin\sigma_M^d = 0$ does not cause the divergence of $\dot{\sigma}_M^d$. Furthermore, it has already been confirmed that the derivative of sigmoid function, $d(\mathrm{sgmf}(z_1))/dz_1$, is bounded as shown in (3.17). Therefore, there exists no singularity problem in the term $\dot{\sigma}_M^d$. In the proposed guidance law, to conclude, there is no non-computable term that could deteriorate the guidance performance drastically.

3.3.2 Stability analysis

In order to verify the stability of the closed-loop dynamics in (3.20), let us consider the Lyapunov candidate function as

$$V = \frac{1}{2}z_1^2 + \frac{\beta^2}{2}z_2^2. \tag{3.29}$$

where β is the positive constant which acts as a scaling factor. Now, the stability of the Lyapunov candidate function in (3.29) can be analyzed as follows.

Theorem 3.2. *Consider the error dynamics (3.20) and the Lyapunov candidate function V in (3.29). Given any $\eta > 0$, for all initial conditions satisfying $V(0) \leq \eta$, there exists a controller gain k_2 such that $V(t) \leq \eta$ $\forall t \geq 0$ and the error signals z_1 and z_2 can be made to converge to zero eventually.*

Proof. For the proof, let us consider the compact set $\mathbb{A} := \{(z_1, z_2) : z_1^2 + \beta^2 z_2^2 \leq 2\eta\}$ such as [49]. Then, $|z_1|$ and $|z_2|$ have maximum values, say $z_1^{\max}$ and $z_2^{\max}$ respectively on $\mathbb{A}$.

Besides, taking the time derivative to the defined candidate function in (3.29) leads to

$$\dot{V} = z_1 \dot{z}_1 + \beta^2 z_2 \dot{z}_2. \tag{3.30}$$

Substituting the closed-loop dynamics (3.20) into (3.30) gives

$$\dot{V} = -k_1 V_M \mathrm{sgmf}(z_1) z_1 - \beta^2 k_2 \left| z_2 \right| + V_M \frac{\cos \sigma_M - \cos \sigma_M^d}{\sigma_M - \sigma_M^d} z_1 z_2. \tag{3.31}$$

In (3.31), the term $(\cos \sigma_M - \cos \sigma_M^d)/(\sigma_M - \sigma_M^d)$ satisfies that

$$\begin{aligned} \left| \frac{\cos \sigma_M - \cos \sigma_M^d}{\sigma_M - \sigma_M^d} \right| &= \left| \frac{(\cos(\sigma_M - \sigma_M^d) - 1) \cos \sigma_M^d - \sin(\sigma_M - \sigma_M^d) \sin \sigma_M^d}{\sigma_M - \sigma_M^d} \right| \\ &\leq \frac{\sqrt{\left\{ \left(\cos(\sigma_M - \sigma_M^d) - 1 \right)^2 + \sin^2(\sigma_M - \sigma_M^d) \right\} \left\{ \cos^2 \sigma_M^d + \sin^2 \sigma_M^d \right\}}}{\left| \sigma_M - \sigma_M^d \right|} \\ &= \frac{\left| 2 \sin \left(\frac{\sigma_M - \sigma_M^d}{2} \right) \right|}{\left| \sigma_M - \sigma_M^d \right|} \leq 1. \end{aligned} \tag{3.32}$$

Substituting the result of (3.32) and the property of $|z_i| \leq z_i^{\max}\ \forall i \in \{1, 2\}$ on $V(z_1, z_2) = \eta$ into (3.31) yields

$$\dot{V} \leq -k_1 V_M \mathrm{sgmf}(z_1) z_1 - \beta^2 |z_2| \left(k_2 - \frac{V_M z_1^{\max}}{\beta^2} \right) \tag{3.33}$$

Since the term $\mathrm{sgmf}(z_1) z_1$ is a positive definite function of the variable z_1, it follows that

$$\dot{V} < 0 \quad \forall\, (z_1, z_2) \in \mathbb{A} - \{\mathbf{0}\} \tag{3.34}$$

if the gain k_2 satisfies $k_2 > V_M z_1^{\max}/\beta^2$. Here, because $z_1^{\max}$ is the maximum value of $|z_1|$ on $\mathbb{A}$, we have $z_1^{\max} \leq \sqrt{2\eta}$. Therefore, let us fix k_2 so as to satisfy $k_2 > V_M \sqrt{2\eta}/\beta^2$ for achieving (3.34). Then, $V \leq \eta$ is an invariant set, i.e., $V(t) \leq \eta\ \forall t > 0$ when $V(t = 0) \leq \eta$. Therefore, the inequality (3.34) holds for all $V(0) \leq \eta$ and all $t > 0$. Furthermore, (3.34)

indicates that the error variables z_1 and z_2 will approach to zero as time goes on. As a result, it can be said that the error signals z_1 and z_2 can also be made to converge to zero eventually. □

Theorem 3.2 signifies that (z_1, z_2) in (3.20) converges to the origin. For the impact time control, however, the convergence of z_1 and z_2 in a finite time is required since flight time is limited. Thus, the following two corollaries are supplemented in order to verify the convergence in a finite time.

Corollary 3.1. *The error variable $z_2(t)$ converges to zero at finite time $t_{z_2=0}$ as*

$$t_{z_2=0} = \frac{|z_2(0)|}{k_2}. \tag{3.35}$$

Proof. From Theorem 3.2, we know that $z_2(t)$ converges to zero eventually. Before the convergence, from (3.20b), we have

$$\frac{d}{dt}\left(z_2^2\right) = -2k_2\sqrt{z_2^2} \tag{3.36}$$

Integrating (3.36) over the interval $0 \leq \tau \leq t$ gives the following [43]:

$$|z_2(t)| = -k_2 t + |z_2(0)|, \tag{3.37}$$

which implies that $z_2(t)$ goes to zero at finite time $t_{z_2=0} = |z_2(0)|/k_2$. □

Corollary 3.2. *For any real number $\varepsilon \in (0, \phi)$, the error variable $z_1(t)$ converges within $[-\varepsilon, \varepsilon]$ at a finite time instant $t_{z_1=\varepsilon}$ bounded as*

$$t_{z_1=\varepsilon} \leq \frac{|z_2(0)|}{k_2} + \frac{V_M t_d - R(0) - \phi}{k_1 V_M} + \frac{\phi}{3k_1 V_M}\log\left(\frac{3\phi^2 - \varepsilon^2}{2\varepsilon^2}\right). \tag{3.38}$$

Proof. From Theorem 3.2, the error variable $z_1(t)$ is proven to satisfy $\lim_{t\to\infty} z_1(t) = 0$, which means the following [50]: For any real number $\varepsilon > 0$, there exists a finite time instant $t_{z_1=\varepsilon}$

such that $|z_1(t)| < \varepsilon \ \forall t > t_{z_1=\varepsilon}$. Also, $t_{z_1=\varepsilon}$ can be selected to satisfy $|z_1(t_{z_1=\varepsilon})| = \varepsilon$ by *intermediate value theorem* since $z_1(t)$ is continuous as shown in (3.12a) and (3.13a).

Then, in order to investigate the finite time $t_{z_1=\varepsilon}$, let us divide the time interval $[0, t_{z_1=\varepsilon}]$ with respect to the properties of z_1 and z_2 as follows:

$$\begin{cases} z_1 > \phi, \ z_2 \neq 0 & \text{for} \ \ 0 \leq t < t_{z_2=0} & (3.39a) \\ z_1 > \phi, \ z_2 = 0 & \text{for} \ \ t_{z_2=0} \leq t < t_{z_1=\phi} & (3.39b) \\ z_1 \leq \phi, \ z_2 = 0 & \text{for} \ \ t_{z_1=\phi} \leq t \leq t_{z_1=z_{1,f}} & (3.39c) \end{cases}$$

where $t_{z_2=0}$ is the reaching time of z_2 defined in Corollary 3.1 and $t_{z_1=\phi}$ is the time when $z_1 = \phi$. Since z_1 is monotone decreasing, $t_{z_1=\phi}$ is unique. The positive constant ϕ is the controller parameter in the sigmoid function of (16) such that $z_1(t) = \phi$ is the moment when the sigmoid function is changed from the signum function to the polynomial form.

First, $[0, t_{z_2=0}]$, the time interval for the convergence of z_2, is obtained as (3.35) in Corollary 2.1. Next, the interval $[t_{z_2=0}, t_{z_1=\phi}]$ has the following relationship:

$$\begin{aligned} t_{z_1=\phi} - t_{z_2=0} &= \int_{t_{z_2=0}}^{t_{z_1=\phi}} \frac{dz_1}{\dot{z}_1} = \frac{z_1(t_{z_1=\phi}) - z_1(t_{z_2=0})}{-k_1 V_M} \\ &\leq \frac{z_1(0) - \phi}{k_1 V_M} = \frac{V_M t_d - R(0) - \phi}{k_1 V_M}. \end{aligned} \tag{3.40}$$

Finally, from (3.16), z_1 dynamics in the interval $[t_{z_1=\phi}, t_{z_1=\varepsilon}]$ is written as

$$\dot{z}_1 = \frac{k_1 V_M}{2\phi^3} z_1 \left(z_1^2 - 3\phi^2 \right), \tag{3.41}$$

and the boundary conditions are given by

$$z_1(t_{z_1=\phi}) = \phi, \quad z_1(t_{z_1=\varepsilon}) = \varepsilon \tag{3.42}$$

where non-negativity of $z_1(t)$ proved by Theorem 3.1 is used. From (3.41) and (3.42), the

solution of $z_1(t)$ in the interval $[t_{z_1=\phi}, t_{z_1=\varepsilon}]$ is expressed as

$$z_1(t) = \frac{\sqrt{3}\phi}{\sqrt{1 + 2\exp\left\{\frac{3k_1V_M}{\phi}\left(t - t_{z_1=\phi}\right)\right\}}}, \tag{3.43}$$

and from (3.43), the interval $[t_{z_1=\phi}, t_{z_1=\varepsilon}]$ is obtained as

$$t_{z_1=\varepsilon} - t_{z_1=\phi} = \frac{\phi}{3k_1V_M}\log\left(\frac{3\phi^2 - \varepsilon^2}{2\varepsilon^2}\right). \tag{3.44}$$

To put together (3.35), (3.40) and (3.44), the reaching time of z_1, which is equivalent to the convergence time within $[-\varepsilon, \varepsilon]$, has the following relationship:

$$\begin{aligned} t_{z_1=\varepsilon} &= t_{z_2=0} + (t_{z_1=\phi} - t_{z_2=0}) + (t_{z_1=\varepsilon} - t_{z_1=\phi}) \\ &\leq \frac{|z_2(0)|}{k_2} + \frac{V_M t_d - R(0) - \phi}{k_1V_M} + \frac{\phi}{3k_1V_M}\log\left(\frac{3\phi^2 - \varepsilon^2}{2\varepsilon^2}\right). \end{aligned} \tag{3.45}$$

which proves Corollary 3.2. □

Corollary 3.1 and 3.2 verify that the proposed guidance law in (3.14) achieves $|z_1| \leq \varepsilon$ and $z_2 = 0$ in a finite time for any small value of $\varepsilon > 0$. Therefore, the homing and impact time conditions in (3.5) and (3.8) can be satisfied under the guidance law in (3.14).

3.3.3 Look-angle analysis

In this subsection, it is confirmed that the look-angle under the proposed law does not exceed the prespecified value by checking whether the FOV limits condition in (3.9) is satisfied. In order to verify the condition in (3.9), let us analyze the dynamics of the missile look angle σ_M.

Theorem 3.3. *Consider the closed-loop dynamics (3.20b) and the controller gain k_1 sat-*

isfying

$$0 \leq k_1 \leq 1 - \cos \sigma_M^{\max} - \varepsilon_1 \tag{3.46}$$

where ε_1 is the positive constant smaller than $1 - \cos \sigma_M^{\max}$. For all initial conditions satisfying $|\sigma_M(0)| \leq \sigma_M^{\max}$, there exists a controller gain k_2 such that $|\sigma_M(t)| \leq \sigma_M^{\max}$ for all $t \geq 0$.

Proof. Let us consider the compact set $\mathbb{B} := \{\sigma_M : |\sigma_M| \leq \sigma_M^{\max}\}$. Then, in the set $\mathbb{B}$, the following always holds:

$$|\sigma_M| \leq \sigma_M^{\max}. \tag{3.47}$$

Also, because z_1 is non-negative as proven in Theorem 3.1 and σ_M^d is defined as (3.14a), we have

$$\cos \sigma_M^d = 1 - k_1 \mathrm{sgmf}(z_1) \leq 1 \tag{3.48a}$$

$$\cos \sigma_M^d = 1 - k_1 \mathrm{sgmf}(z_1) \geq 1 - k_1 \tag{3.48b}$$

where the property $0 \leq \mathrm{sgmf}(z_1) \leq 1$ for $z_1 \geq 0$ shown in (3.16) and (3.17a) are used. Then, from (3.46) and (3.48), $\cos \sigma_M^d$ satisfies

$$\cos \sigma_M^{\max} + \varepsilon_1 \leq \cos \sigma_M^d \leq 1, \tag{3.49}$$

which leads to

$$\cos^{-1}(1) \leq \left|\sigma_M^d\right| \leq \cos^{-1}\left(\cos \sigma_M^{\max} + \varepsilon_1\right). \tag{3.50}$$

Since ε_1 is chosen to satisfy $0 < \varepsilon_1 + \cos\sigma_M^{\max} < 1$ as described after (3.46), we obtain

$$\begin{aligned} 0 \leq \left|\sigma_M^d\right| &\leq \cos^{-1}\left(\cos\sigma_M^{\max} + \varepsilon_1\right) \\ &< \cos^{-1}\left(\cos\sigma_M^{\max}\right) \\ &= \sigma_M^{\max}. \end{aligned} \tag{3.51}$$

Now, for the proof of Theorem 3.3, consider the square function of the look angle as

$$V_{\sigma_M} = \frac{1}{2}\sigma_M^2. \tag{3.52}$$

From (3.15), taking the time derivative to the above V_{σ_M} in (3.52) leads to

$$\begin{aligned} \dot{V}_{\sigma_M} &= \sigma_M\left(\frac{a_M}{V_M} - \dot{\lambda}\right) \\ &= \sigma_M\left(-k_2\mathrm{sgn}(z_2) + \dot{\sigma}_M^d\right) \end{aligned} \tag{3.53}$$

From (3.26), the term $\dot{\sigma}_M^d$ in (3.53) is expressed as

$$\dot{\sigma}_M^d = -k_1 V_M \frac{1-\cos\sigma_M}{\sin\sigma_M^d}\frac{d}{dz_1}\mathrm{sgmf}(z_1) \tag{3.54}$$

Here, the term $\left(1-\cos\sigma_M\right)/\sin\sigma_M^d$ is continuous for all σ_M and σ_M^d satisfying (3.47) and (3.51) because the result in (3.28) implies the continuity at $\sin\sigma_M^d = 0$. Therefore, from *extreme value theorem*, the term $(1-\cos\sigma_M)/\sin\sigma_M^d$ has minimum and maximum values in the set $\mathbb{B}$. In addition, the term $d(\mathrm{sgmf}(z_1))/dz_1$ is always bounded as shown in (3.17). In summary, there exists a positive constant $\dot{\sigma}_M^{d,\max}$ that satisfies

$$\left|\dot{\sigma}_M^d\right| \leq \dot{\sigma}_M^{d,\max} \tag{3.55}$$

Now, on $\sigma_M = \sigma_M^{\max}$, $\dot{V}_{\sigma_M}$ in (3.53) has the following relationship:

$$\dot{V}_{\sigma_M}\Big|_{\sigma_M=\sigma_M^{\max}} \leq -\sigma_M^{\max}\left\{k_2 \mathrm{sgn}(\sigma_M^{\max} - \sigma_M^d) - \dot{\sigma}_M^{d,\max}\right\} \tag{3.56}$$

The selection of the gain k_2 satisfying $k_2 > \dot{\sigma}_M^{d,\max}$ yields

$$\dot{V}_{\sigma_M}\Big|_{\sigma_M=\sigma_M^{\max}} \leq 0. \tag{3.57}$$

Likewise, on $\sigma_M = -\sigma_M^{\max}$, we obtain

$$\begin{aligned}\dot{V}_{\sigma_M}\Big|_{\sigma_M=-\sigma_M^{\max}} &\leq -\sigma_M^{\max}\left\{k_2 \mathrm{sgn}(\sigma_M^{\max} + \sigma_M^d) - \dot{\sigma}_M^{d,\max}\right\} \\ &\leq 0. \end{aligned} \tag{3.58}$$

As a result, $|\sigma_M(t)| \leq \sigma_M^{\max}$ is an invariant set under the proposed law, which means $|\sigma_M(t)| \leq \sigma_M^{\max}\ \forall\ t \geq 0$. □

From Theorem 3.3, it can be verified that the look angle σ_M achieves $|\sigma_M(t)| \leq \sigma_M^{\max}$ for the initial condition satisfying $|\sigma_M(0)| \leq \sigma_M^{\max}$ under the choice of k_1 such as (3.46) and k_2 satisfying $k_2 > \dot{\sigma}_M^{d,\max}$. This result implies that the condition for FOV limits in (3.9) can be fulfilled. To conclude, the proposed guidance law can prevent the violation of the prespecified FOV limits during the homing.

3.3.4 Discussion about achievable impact time

In common missile guidance problems in which the interceptor's longitudinal acceleration is unavailable, the achievable impact time is physically restrictive. Particularly, because of the consideration of the FOV limits, the restriction becomes severe in this problem compared with other approaches that do not take into account the FOV limits. In this regard, the discussion about achievable impact time under the proposed law is helpful for

real applications.

In virtue of the look angle limits, the closing velocity is also confined under the proposed law, so a simple necessary condition for the achievable desired impact time can be calculated as follows:

$$\frac{R(0)}{V_M} = \frac{R(0)}{|V_R|_{\max}} \leq t_d \leq \frac{R(0)}{|V_R|_{\min}} = \frac{R(0)}{V_M \cos \sigma_M^{\max}} \tag{3.59}$$

Namely, in order to fulfill the homing and impact time control simultaneously, the desired impact time should be selected to satisfy the condition in (3.59). However, the satisfaction of (3.59) does not imply the success of the tasks. This subsection investigates the sufficient condition, i.e., the minimum and maximum achievable desired impact times, by analyzing the closed-loop dynamics.

3.3.4.1 minimum achievable impact time

Since the longitudinal acceleration is unavailable in the missile model of this chapter, as commonly assumed in many literature [12–37], the desired time-to-go should be greater than or equal to the remaining time-to-go on the collision course, which can be expressed mathematically as

$$t_{go}^d = (t_d - t) \geq \frac{R}{V_M}. \tag{3.60}$$

The expression in (3.60) is, in fact, equivalent to the condition of $z_1(t) \geq 0$ by definition of z_1, and Theorem 3.1 in the subsection 3.3.1 has already given the sufficient condition for achieving $z_1(t) \geq 0$: the satisfaction of initial condition in (3.25). In other words, the condition in (3.25) is the sufficient condition for obeying (3.60). The expression in (3.25) can be rewritten as

$$t_d > \frac{R(0) + z_{1,f}}{V_M} + \frac{2\,|z_2(0)|}{k_2}, \tag{3.61}$$

which means that the proposed guidance law can achieve any desired impact time greater than the right-hand side of (3.61) and smaller than the maximum achievable impact time to be analyzed in the next subsection.

3.3.4.2 maximum achievable impact time

In the process of analyzing the minimum achievable impact time in the subsection 3.3.4.1, the property that z_1 should converge more slowly than z_2 in order to satisfy (3.60) was utilized. For analyzing the maximum achievable impact time, the similar concept is also used. As explained in the section 3.2.1, the convergence of z_1 and z_2 in a finite time enables the missile to intercept the target at the desired impact time. In other words, the convergence of z_1 and z_2 before the desired impact time suffices. From Corollary 3.1, it is known that the convergence time of z_2 can be decreased deliberately by adjusting the gain k_2. On the contrary, it is difficult to freely reduce the convergence time of z_1 because Corollary 3.2 shows that $t_{z_1=\varepsilon}$ in (3.38) is determined dominantly by the gain k_1 whose maximum bounds are restricted as given by (3.46). Therefore, the convergence time of z_1 is focused to consider the maximum achievable impact time.

In the section 3.3.1, $z_{1,f}$ is defined as the maximum acceptable error of z_1, which is obtained by (3.12a) with the maximum allowable miss distance. That is, substituting $\varepsilon = z_{1,f}$ in (3.38), the maximum bounds of the convergence time for achieving $|z_1(t)| \leq z_{1,f}$ can be calculated as follows:

$$t_{z_1=z_{1,f}} \leq \frac{|z_2(0)|}{k_2} + \frac{V_M t_d - R(0) - \phi}{k_1 V_M} + \frac{\phi}{3k_1 V_M} \log\left(\frac{3\phi^2 - z_{1,f}^2}{2z_{1,f}^2}\right) \tag{3.62}$$

where $t_{z_1=z_{1,f}}$ is the convergence time for $|z_1(t)| \leq z_{1,f}$. Then, the sufficient condition for preventing the desired impact time from exceeding the maximum achievable impact time

is given by

$$
\begin{aligned}
t_{z_1=z_{1,f}} \leq & \frac{|z_2(0)|}{k_2} + \frac{V_M t_d - R(0) - \phi}{k_1 V_M} + \frac{\phi}{3k_1 V_M} \log\left(\frac{3\phi^2 - z_{1,f}^2}{2z_{1,f}^2}\right) \\
\leq & t_d,
\end{aligned} \tag{3.63}
$$

which is rewritten as

$$
t_d \leq \frac{R(0)+\phi}{V_M(1-k_1)} - \frac{k_1|z_2(0)|}{k_2(1-k_1)} - \frac{\phi}{3V_M(1-k_1)} \log\left(\frac{3\phi^2 - z_{1,f}^2}{2z_{1,f}^2}\right). \tag{3.64}
$$

The result in (3.64) implies that the desired impact time less than or equal to the right-hand side can be achievable if the condition in (3.61) is also satisfied. In conclusion, it can be said that the desired impact time satisfying both (3.61) and (3.64) is sufficiently achieved under the proposed law.

Remark 3.1. *For a given desired impact time t_d, if the controller gain k_1 satisfies (3.64), the impact time constraint can be achieved sufficiently. That is, from (3.64), the sufficient condition about k_1 for achieving a given desired impact time can be deduced. If k_1 is selected as $k_1 = 1 - \cos\sigma_M^{\max} - \varepsilon_1$, the sufficient condition for satisfying (56) is given by*

$$
\cos\sigma_M^{\max} + \varepsilon_1 \leq \frac{R(0)+\phi}{V_M t_d} - \frac{|z_2(0)|}{k_2 t_d} - \frac{\phi}{3V_M t_d} \log\left(\frac{3\phi^2 - z_{1,f}^2}{2z_{1,f}^2}\right), \tag{3.65}
$$

which is rewritten as

$$
\sigma_M^{\max} \geq \cos^{-1}\left(\frac{R(0)+\phi}{V_M t_d} - \frac{|z_2(0)|}{k_2 t_d} - \frac{\phi}{3V_M t_d} \log\left(\frac{3\phi^2 - z_{1,f}^2}{2z_{1,f}^2}\right) - \varepsilon_1\right). \tag{3.66}
$$

This result implies that the given desired impact time t_d can be achieved under the proposed law if the acceptable maximum value of the missile look angle satisfies (3.66).

3.4 SIMULATION RESULTS

In this section, the performance of the proposed guidance law is demonstrated through three subsections involving numerical simulations. Subsection 3.4.1 evaluates the validity of the proposed law in various engagement scenarios against a stationary target. Subsection 3.4.2 compares the proposed law with other guidance laws that take into account the constraint on impact time. To examine the performance in realistic applications, subsection 3.4.3 carries out a salvo attack simulation with a realistic interceptor model.

When the proposed law is applied, the signum function $\mathrm{sgn}(\cdot)$ in the command may produce undesirable chattering due to the discontinuity. To alleviate this problem and generate acceptable guidance command, the signum function in the control component in (3.15b) is approximated by the continuous sigmoid function used in [10] as follows:

$$\mathrm{sgmf}_2(x) = 2\left(\frac{1}{1+\exp^{-ax}} - \frac{1}{2}\right), \quad a > 0. \tag{3.67}$$

Such an approximation enables the convergence with slight deviation from the ideal sliding mode. As verified in [44], the deviation is inversely proportional to the parameter a approximately, and a is selected as 10 in this work.

The acceleration command of the missile is confined within $\pm 10\ g$ where g represents

Table 3.1: Simulation setting

Parameters	Values
Initial missile position $(x_M(0), y_M(0))$	$(0, 0)$ km
Stationary target position $(x_T(0), y_T(0))$	$(10, 0)$ km
Initial missile flight path angle $\gamma_M(0)$	30 deg
Missile speed V_M	250 m/s
Missile acceleration limits $\lvert a_M\rvert^{\max}$	10 $g^{\dagger}$
look angle limits $\sigma_M^{\max}$	50, 60°
Controller gains	$k_1 = 1 - \cos\sigma_M^{\max} - 10^{-3},\ k_2 = 1$ $\phi = 200$

† g denotes the acceleration of gravity, i.e., $g = 9.81$ m/s^2.

the gravitational acceleration and the simulations are terminated when the relative range is less than or equal to 0.1 m in all the engagements. The controller gains used in the simulations are listed in TABLE. 3.1.

3.4.1 Performance analysis of the proposed law

This subsection demonstrates the performance of the proposed guidance law by conducting numerical simulations which involve various engagement scenarios. With various desired impact times and two different look angle limitations, the detailed parameter values used in simulations are listed in TABLE. 3.1. In all the simulations, the engagement terminates when the relative range R is less than 0.1 m.

Figure 3.2 shows the simulations results for three different impact time constraints with look angle limitation of $\sigma_M^{\max} = 50°$. The results for the desired impact times of $t_d^{\min}(= 40.68 \text{ s})$, 50 s and $t_d^{\max}(= 54.06 \text{ s})$ are illustrated by the triangle-patterned-line, inverted triangle-patterned-line and square-patterned-line respectively. The minimum and maximum achievable impact times of $t_d^{\min}$ and $t_d^{\max}$ are calculated to satisfy (3.61) and (3.64) where $z_{1,f}$, the maximum acceptable error of z_1, is selected as $z_{1,f} = 0.01$.

As illustrated by Fig. 3.2a, the proposed guidance law achieves the interception of the stationary target for all three cases. The terminal impact time errors in all three cases satisfy $|t_f - t_d| \leq 1 \times 10^{-3}$ sec.

Figure 3.2b shows the convergence of z_1 and z_2 which guarantees the accomplishment of the interception of the target at the desired impact time as verified in section 3.2.2. Especially, the convergence of z_1 and z_2 is achieved when $t_d = t_d^{\min}$ and $t_d = t_d^{\max}$, which gives validity to the analysis of achievable impact time investigated in section 3.3.4.

As expected, the upper plot of figure 3.2a shows that the missile makes a longer detour as the desired impact time increases. This results in the increase of the look angle, but the look angle does not exceed the prescribed value as proved in the section 3.3.3 and confirmed in fig. 3.2c.

Figure 3.3 provides the results for four different values of impact time constraints with

the look angle limitation of $\sigma_M^{\max} = 60°$. Likewise, the results for the impact time constraints of $t_d^{\min}(= 41.03$ s), 50 s, 60 s and $t_d^{\max}(= 68.93$ s) are denoted by the triangle, inverted triangle, square and circle-patterned-line respectively. Similar to the results in Fig. 3.2, the minimum and maximum achievable impact times $t_d^{\min}$ and $t_d^{\max}$ are determined to satisfy the conditions (3.61) and (3.64). We can see that the maximum achievable impact time $t_d^{\max}$ of this case when $\sigma_M^{\max} = 60°$ is increased compared with $t_d^{\max}$ of the case when $\sigma_M^{\max} = 50°$. It is physically obvious because the limitation of detour curvature is alleviated as the maximum possible look angle increases. Mathematically, the increase of $t_d^{\max}$ results from following the increased $\sigma_M^{\max}$ which determines the right-hand side of (3.64).

Figure 3.3a demonstrates that the proposed guidance law fulfills the interception of the target for all four cases. Furthermore, the resulting impact time errors in all the cases satisfy $|t_f| \leq 1 \times 10^{-3}$. That is, it can be said that the proposed law achieves the impact time control for every considered case.

Similar to Fig. 3.2b, figure 3.3b shows the convergence of z_1 and z_2, which verifies the fulfillment of the impact time control theoretically. Furthermore, the discussion about minimum and maximum achievable domain of impact time , given in 3.3.4, is demonstrated by the results about the convergence of z_1 and z_2 when $t_d = t_d^{\min}$ and $t_d = t_d^{\max}$.

The look angle histories in Fig. 3.3c also show that the proposed law prevents the missile from violating the pre-set FOV limit. We can observe that the look angle does not exceed the prespecified value of 60° for every considered case. This property about look angle restriction is shown noticeably compared with other existing impact time control guidance law, which will be given by next subsection 3.4.2.

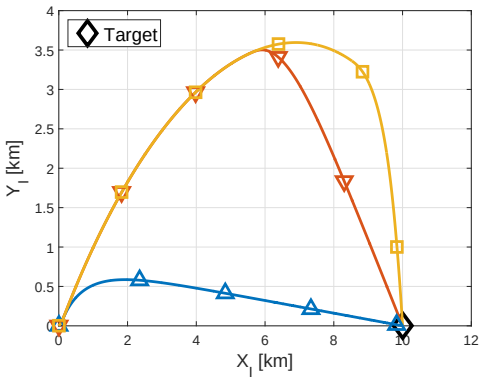

(a) Flight trajectories for $\sigma_M^{\max} = 50°$

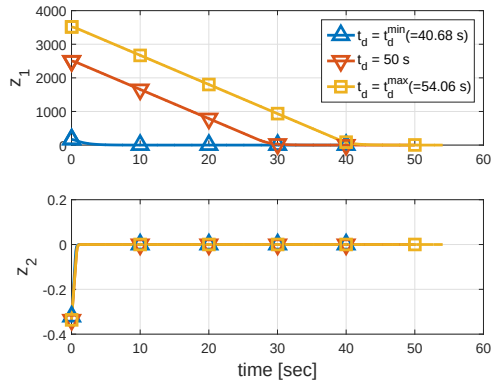

(b) Error variables for $\sigma_M^{\max} = 50°$

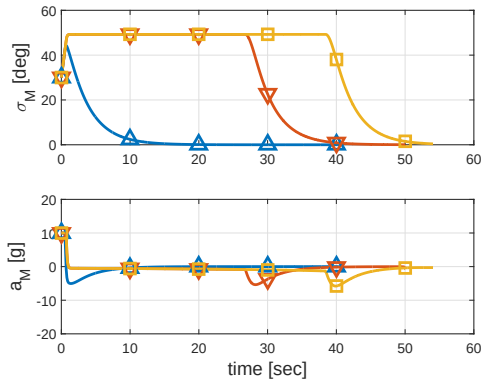

(c) Look angles and guidance commands for $\sigma_M^{\max} = 50°$

Figure 3.2: Simulation results for different impact time constraints with look angle limitation of $\sigma_M^{\max} = 50°$: triangle-patterned-line, inverted triangle-patterned-line and square-patterned-line represent the results for $t_d = t_d^{\min}(= 40.68\ s)$, $50\ s$ and $t_d^{\max}(= 54.06\ s)$ respectively.

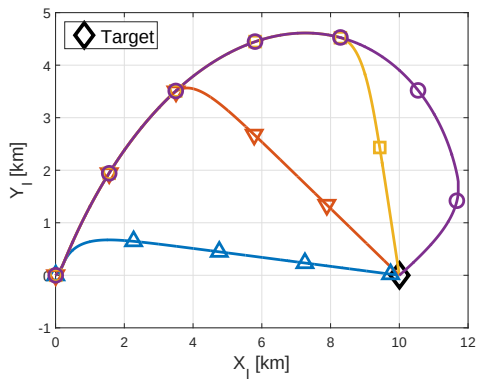

(a) Flight trajectories for $\sigma_M^{\max} = 60°$

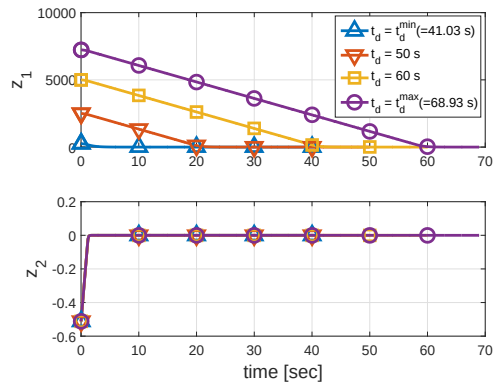

(b) Error variables for $\sigma_M^{\max} = 60°$

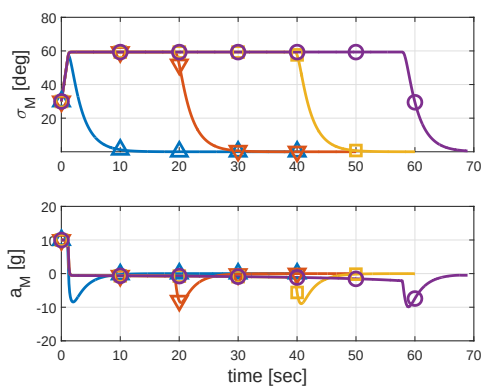

(c) Look angles and guidance commands for $\sigma_M^{\max} = 60°$

Figure 3.3: Simulation results for different impact time constraints with look angle limitation of $\sigma_M^{\max} = 60°$: triangle-patterned-line, inverted triangle-patterned-line, square-patterned-line and circle-patterned-line represent the results for $t_d = t_d^{\min}(= 41.03\ s)$, $50\ s$, $60\ s$ and $t_d^{\max}(= 68.93\ s)$ respectively.

3.4.2 Performance comparison with other guidance laws

For an effective analysis of the proposed guidance law, the performance is compared with other existing laws that aim to control impact time against a stationary target called Lya-ITCG (lyapunov-based impact time control guidance law) and PN-ITCG (proportional navigation-based impact time control guidance law) represented in [25] and [30] respectively. As an engagement scenario, the same initial condition considered in 3.4.1 are used with the desired impact time of 60 s. The desired constraint of look angle is fixed as $\sigma_M^{\max} = 60°$.

Lya-ITCG can guarantee a wide range of the capture region with an acceptable command owing to its exact nonlinear formulation, so this law is suitable for engagements requiring large heading angle errors. PN-ITCG is appropriate when maneuverable energy of the missile is restricted because it is designed to minimize the guidance effort based on the optimal control theory. However, when the missile is equipped with the seeker with reduced FOV, these two laws have difficulty fulfilling the homing since the constraint about reduced FOV is not considered. In particular, the difficulty becomes severe when an engagement requires a large detour to satisfy the desired impact time constraint. This subsection illustrates such an engagement in fig. 3.4.

Figure 3.4 shows the simulation results for $t_d = 60$ s under three different guidance laws. The results under Lya-ITCG, PN-ITCG and proposed law are illustrated by the triangle, inverted triangle and square-patterned-line respectively. As shown in Fig. 3.4a, all the three guidance laws achieve the interception of the stationary target. The terminal impact time errors in all three cases satisfy $|t_f - t_d| \leq 1 \times 10^{-3}$ sec.

In order to fulfill the impact time control, all three laws let the missile make a detour, which results in the increase of the look angle in the initial phase as illustrated in 3.4b. Particularly, the look angles under Lya-ITCG and PN-ITCG increase to about 119° and 78° respectively exceeding $\sigma_M^{\max} = 60°$, which may cause the missile seeker to lose the target. In comparison, it can be seen that the look angle under the proposed law does not exceed the prescribed value until the interception although its magnitude approaches maximum

limit. Hence, it can be confirmed that the proposed law can prevent the violation of the FOV limits.

Figure 3.4c represents the guidance commands under three guidance laws. Owing to its optimality of PN component, PN-ITCG generates the acceleration command of modest amplitude during the entire homing. On the contrary, Lya-ITCG and the proposed law generate a large command in the initial phase due to requiring the convergence of error. Furthermore, the proposed law generates a large command once more in the middle phase. It is related with earlier convergence of $\sigma_M = 0$ than other laws.

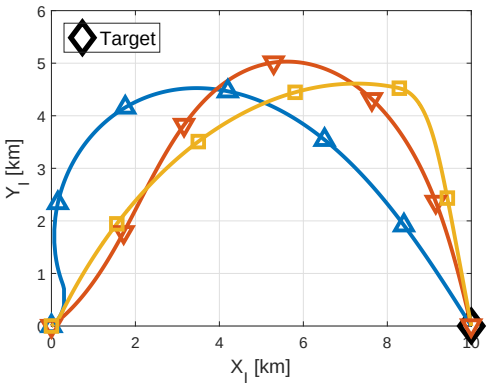

(a) Flight trajectories for $t_d = 60$ s

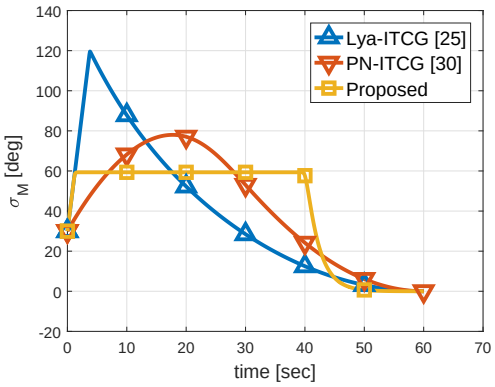

(b) Look angles for $t_d = 60$ s

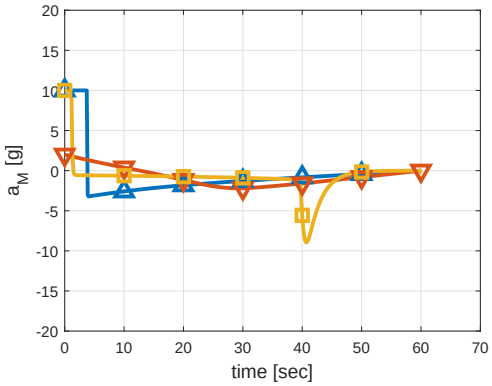

(c) Guidance commands for $t_d = 60$ s

Figure 3.4: Simulation results for impact time constraint of 60 s under different guidance laws: triangle-patterned-line, inverted triangle-patterned-line and square-patterned-line represent the results of Lya-ITCG, PN-ITCG and proposed law respectively.

3.4.3 Salvo attack in a realistic engagement

Although the proposed guidance law is derived with the assumption of constant missile speed, real implementations require the consideration of time-varying speed because of aerodynamic and gravitational effects. Therefore, it is necessary to check the achievement of the desired duties such as homing and impact time control under the proposed law in more realistic settings. To confirm the performance of the law more unquestionably, this subsection conducts the salvo attack simulation that takes into account the realistic interceptor model first introduced in [51] and utilized in [26].

Considering the thrust, aerodynamics and gravitation, the missile speed varies with

$$\dot{V}_M = \frac{T - D}{m} - g \sin \gamma_M \tag{3.68}$$

and the dynamics of flight path angle in (3.3) is replaced by

$$\dot{\gamma}_M = \frac{a_M - g \cos \gamma_M}{V_M} \tag{3.69}$$

where T is the longitudinal thrust, D the aerodynamic drag force, m the missile mass, and g the gravitational acceleration respectively. To model the boost phase with a fuel-injection

Table 3.2: Simulation setting for salvo attack

	$M1$	$M2$	$M3$	$M4$
Initial position $(x_M(0), y_M(0))$	$(0, 0)$ km	$(-2, 1)$ km	$(2, -3)$ km	$(19, -2)$ km
Initial flight path angle $\gamma_M(0)$	$30°$	$20°$	$70°$	$150°$
Initial speed $V_M(0)$	250 m/s	270 m/s	280 m/s	240 m/s
Acceleration limits $\lvert a_M \rvert^{\max}$			$10\ g$	
Desired impact time t_d			50 sec	
Look angle limits $\sigma_M^{\max}$			$60°$	

at the initial stage, the thrust and mass are considered as

$$T = \begin{cases} 33000 & 0 \leq t \leq 1.5 \\ 7500 & 1.5 \leq t \leq 8.5 \\ 0 & 8.5 \leq t \end{cases} \tag{3.70}$$

$$m = \begin{cases} 135 - 14.53t & 0 \leq t \leq 1.5 \\ 113.205 - 3.31t & 1.5 \leq t \leq 8.5 \\ 90.035 & 8.5 \leq t \end{cases} \cdot \tag{3.71}$$

The drag is modeled as

$$D = C_{D0} Q S_{ref} + \frac{K_i m^2 a_M^2}{Q S_{ref}} \tag{3.72}$$

where C_{D0}, K_i, Q and S_{ref} denote the zero-lift drag coefficient, induced drag coefficient, dynamic pressure and reference area respectively. The exact values and expressions of these parameters and variables are included in [51].

In addition to the velocity model in (3.68)∼(3.72), it is also assumed that the lateral maneuvering acceleration a_M is generated by the aerodynamic lift force as

$$a_M = \frac{L(\alpha, \delta)}{m} \tag{3.73}$$

and the rotational motion is given by

$$\begin{aligned} \dot{\alpha} =& q - \frac{L(\alpha, \delta)}{m V_M}, \quad \dot{\theta} = q \\ \dot{q} =& \frac{M(\alpha, q, \delta)}{I_{yy}}, \quad \dot{\delta} = \frac{\delta_C - \delta}{\tau_\delta} \end{aligned} \tag{3.74}$$

where α, θ, q and δ denote the angle of attack, pitch angle, pitch rate and canard deflection angle respectively. $L(\cdot)$ and $M(\cdot)$ represent the lift force and pitching moment, and m and

I_{yy} are the mass and moment of inertia with respect to the pitch axis. δ_C and τ_δ represent the command of the canard deflection angle and time constant of the actuator dynamics. As specific expressions for the lift force $L(\cdot)$ and pitch moment $M(\cdot)$, the aerodynamic model used in [45] and [9] is applied.

Using the realistic model described above, the salvo attack scenario in which four missiles denoted as $M1$, $M2$, $M3$ and $M4$ respectively are employed against a single stationary target located at $(10, 0)$ km is performed. The specific initial values of the missiles are listed in TABLE. 3.2.

Figure 3.5 provides the simulation results for the salvo attack. The results of $M1$, $M2$, $M3$ and $M4$ are represented by the triangle-patterned-line, inverted triangle-patterned-line, square-patterned-line and circle-patterned-line respectively. First of all, figure 3.5a shows that all four missiles intercept the stationary target. Furthermore, the terminal impact times of missiles $M1 \sim 4$ are 50.039 s, 49.980 s, 50.041 s and 50.050 s respectively, which indicates the impact time error is within 5×10^{-2} s for every missile.

Due to the consideration of boost phase, we can observe that the speeds of missiles rise steeply at the initial stage as shown in Fig. 3.5c, and decrease after the fuel injection is finished because the drag is applied dominantly.

Although this variation of the speed is not involved in the guidance law design, figure 3.5b shows that the proposed law satisfies the constraint of FOV limit for every missile. It is because the selection of gain k_2 with large enough value can allow the missile look angle not to exceed the prescribed value as shown in (3.56) and (3.58) despite the presence of uncertainties. In conclusion, the proposed law holds the validity in spite of the presence of undesigned effects: the variation of the speed in this case.

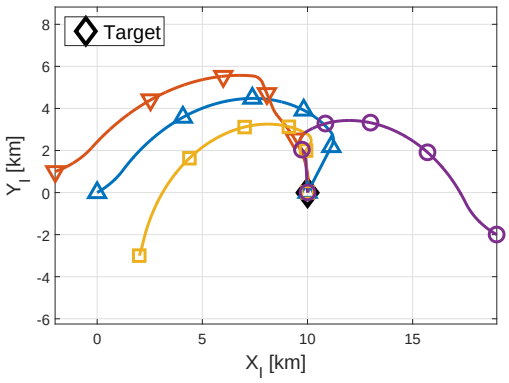

(a) Flight trajectories for the salvo attack

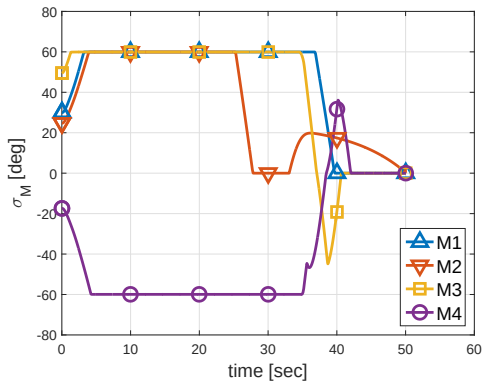

(b) Look angles for the salvo attack

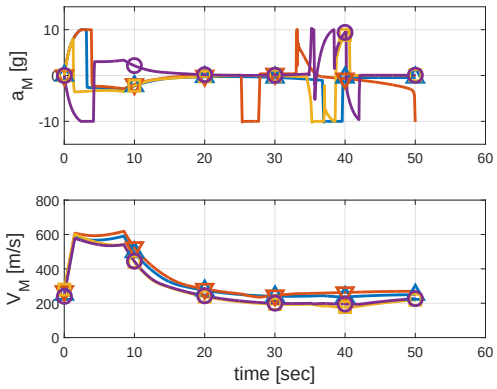

(c) Guidance commands and speeds for the salvo attack

Figure 3.5: Simulation results for the salvo attack

4

Impact Angle and Time Control Guidance with Field-of-View Constraint

In this chapter, a guidance law that considers the field-of-view limitation as well as the terminal impact angle and time constraints is proposed. In order to develop the guidance law, a desired look angle that satisfies the field-of-view limitation and terminal impact angle constraint is first designed. Since the desired look angle is shaped to involve an additional guidance gain that determines the length of the trajectory, the terminal impact time can be controlled by adjusting the gain. The guidance law is derived so as to stabilize the actual look angle to the desired look angle based on the sliding mode control method. As a result, the proposed law in this chapter can intercept the stationary target at the desired impact angle and time with satisfying the field-of-view constraint. The proposed law is expected to achieve the accurate performance in real applications owing to its analytic formulation without using any numerical routine such as off-line optimization or the shooting method. The effectiveness of the proposed guidance law is demonstrated by numerical simulations.

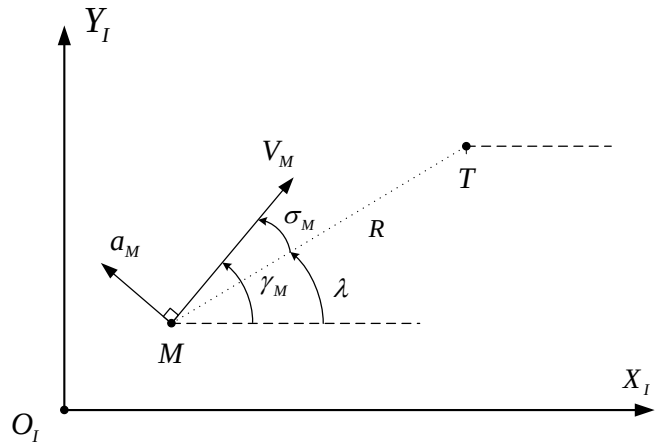

Figure 4.1: Two-dimensional engagement geometry for a stationary target

4.1 Problem formulation

This section states engagement dynamics of a missile against a stationary target in order to set a framework for impact angle and time control guidance. Figure 4.1 shows the two-dimensional engagement geometry of the missile and target denoted by M and T respectively in the inertial frame of $X_I O_I Y_I$. In Fig. 4.1, R and λ represent the relative range and line-of-sight (LOS) angle of the target with respect to the missile. V_M, a_M, γ_M and σ_M denote the speed, normal acceleration, flight path angle and lead angle of the missile respectively. Especially, with the assumption that the angle of attack is small enough to be neglected, σ_M is approximated as the look angle which represents the included angle between the LOS and missile heading. This paper focuses on limiting the look angle σ_M since it mainly determines the viewing angle of the seeker.

The kinematic equations that governs the engagement are given by

$$\dot{R} = V_R \tag{4.1a}$$

$$R\dot{\lambda} = V_\lambda \tag{4.1b}$$

where V_R and V_λ are relative velocity components of the target with respect to the missile.

V_R and V_λ each represent the component along and normal to the LOS respectively as

$$V_R = -V_M \cos\sigma_M \tag{4.2a}$$

$$V_\lambda = -V_M \sin\sigma_M. \tag{4.2b}$$

To steer the desired direction, the missile generates the maneuvering acceleration a_M normal to the velocity vector. Thus, the equations of the flight path angle is expressed as

$$\dot{\gamma}_M = \frac{a_M}{V_M}. \tag{4.3}$$

This paper proposes an impact angle and time control guidance law that prohibits the look angle within the maximum limit, so the design goals are written as

$$\exists\, t_f > 0 : R(t) > 0\ \forall t \in [0, t_f) \text{ and } R(t_f) = 0 \tag{4.4a}$$

$$\gamma_M(t_f) = \gamma_d \tag{4.4b}$$

$$t_f = t_d \tag{4.4c}$$

$$|\sigma_M(t)| \leq \sigma_M^{\max} < \pi/2 \quad \forall t \in [0, t_f] \tag{4.4d}$$

where t_f, γ_d, t_d and $\sigma_M^{\max}$ mean the final time, desired impact angle, desired impact time and prescribed maximum look angle. The conditions in (4.4a), (4.4b), (4.4c) and (4.4d) are related to the homing, impact angle, impact time and field-of-view constraints respectively.

Achieving all these conditions is a difficult problem since only the normal acceleration is used as guidance command. To deal with this problem, a look angle constrained impact angle control guidance law that does not consider the impact time constraint is first designed in section 4.2. This law is extended to an impact angle and time control guidance law based on the calculation of remaining time-to-go in section 4.3.

4.2 Impact angle control guidance law with look angle constraint

In this section, an impact angle control guidance law with a free impact time is designed as the groundwork for developing the guidance law that controls both the impact angle and time. In subsection 4.2.1, a look angle profile that guarantees the interception at the desired impact angle without violating the look angle constraint is first introduced. An impact angle control guidance law that tracks the desired look angle profile is then developed using the lyapunov stability theory in subsection 4.2.2.

4.2.1 Look angle shaping based on nonlinear formulation

Against a stationary target, nullifying the look angle enables the homing of the missile. In addition, approaching the target over the collision path of the desired way ensures the fulfillment of impact angle control. Therefore, the error variable for the impact angle control can be defined as follows:

$$e_1 = \lambda - \gamma_d \tag{4.5}$$

Regulating the error variable e_1 in (4.5) guarantees the interception at the desired impact angle since the collision path in the desired direction is achieved. Differentiating (4.5) with respect to the relative range, we have

$$\frac{de_1}{dR} = \frac{\tan \sigma_M}{R}. \tag{4.6}$$

Based on (4.6), let the desired profile of the look angle be defined as

$$\sigma_M^d = k_1 \text{sat}\left(\frac{e_1}{\phi_1}\right) \tag{4.7}$$

where sat$(\cdot)$ is the saturation function such that sat$(x) = x$ if $|x| \leq 1$ and sat(x) =sgn(x) otherwise. Also, k_1 and ϕ_1 are guidance parameters and chosen to satisfy the followings:

$$0 < k_1 \leq \sigma_M^{\max} < \frac{\pi}{2}, \quad 0 < \phi_1 \tag{4.8}$$

Note that the magnitude of the desired look angle σ_M^d is limited as $\left|\sigma_M^d\right| \leq k_1 \leq \sigma_M^{\max}$. It makes the designed profile be within the maximum limits. From (4.1a) and (4.2a), furthermore, it is deduced that the relative range is strictly decreasing if the look angle is within $(-\pi/2, \pi/2)$. Hence, after achieving $\sigma_M = \sigma_M^d$, the homing and FOV constraints in (4.4a) and (4.4d) can be satisfied. The controller to achieve $\sigma_M = \sigma_M^d$ is designed in next subsection 4.2.2.

Next, it is verified whether the proposed σ_M^d guarantees the satisfaction of impact angle constraint. Substituting (4.7) into (4.6) yields

$$\frac{de_1}{dR} = \begin{cases} \dfrac{\tan k_1}{R} & \text{for } |e_1| > \phi_1 \quad (4.9a) \\ \dfrac{1}{R}\tan\left(\dfrac{k_1}{\phi_1}e_1\right) & \text{for } |e_1| \leq \phi_1 \quad (4.9b) \end{cases}$$

Solving the equations in (4.9a) and (4.9b), we obtain

$$e_1(R) = \begin{cases} e_1(R_0) + \log\left(\dfrac{R}{R_0}\right)^{\tan k_1} & \text{for } |e_1| > \phi_1 \quad (4.10a) \\ \dfrac{\phi_1}{k_1}\sin^{-1}\left\{\sin\left(\dfrac{k_1}{\phi_1}e_1(R_1)\right)\left(\dfrac{R}{R_1}\right)^{k_1/\phi_1}\right\} & \text{for } |e_1| \leq \phi_1 \quad (4.10b) \end{cases}$$

where R_0 and R_1 are relative ranges at the beginning of each interval, i.e., $R_0 = R(t = 0)$ and $|e_1(R_1)| = \phi_1$. The solutions in (4.10a) and (4.10b) shows that e_1 is strictly decreasing since R is also strictly decreasing. Furthermore, (4.10b) indicates that e_1 goes to zero when $R = 0$. As a result, the proposed look angle profile in (4.7) guarantees that the missile intercepts the target at the designated impact angle without violating the maximum look angle constraint.

Note that the desired tasks in (4.4a), (4.4b) and (4.4d) are guaranteed regardless of the magnitude of ϕ_1 which determines the look angle profile as shown in (4.7). This parameter ϕ_1 is utilized to achieve the desired impact time in the section 4.3

4.2.2 Design of the guidance law to follow the look angle profile

To substantialize the property of the designed profile σ_M^d, it is necessary to make the actual look angle σ_M converge to σ_M^d. In this subsection, the controller that achieves the convergence is derived based on the sliding mode technique. A sliding surface variable to track the desired look angle is defined as

$$S = \sigma_M - \sigma_M^d. \tag{4.11}$$

Taking the time derivative to (4.11) yields

$$\dot{S} = \frac{a_M}{V_M} - \dot{\lambda} - \dot{\sigma}_M^d. \tag{4.12}$$

From (4.12), a sliding mode guidance law that stabilizes S at zero is designed as follows:

$$a_M = V_M \left(\dot{\lambda} + \dot{\sigma}_M^d \right) - k_2 V_M \mathrm{sgn}(S) \tag{4.13}$$

where k_2 is a positive constant that determines the convergence speed of S. Since the closed loop dynamics of S under applying the guidance law in (4.13) is given by

$$\dot{S} = -k_2 \mathrm{sgn}\left(S\right), \tag{4.14}$$

the sliding mode is achieved in a finite time t_r as follows [43]:

$$t_r = \frac{|S(0)|}{k_2} \tag{4.15}$$

In order to fulfill the desired tasks, the surface variable S has to converge before the interception. Therefore, the reaching time t_r should be faster than the final time t_f, so the parameter k_2 should be chosen to satisfy

$$k_2 \geq \frac{|S(0)|}{t_f}. \tag{4.16}$$

Then, the proposed guidance law in (4.13) guarantees the interception at the desired impact angle since the actual look angle tracks the designed look angle profile in (4.7) before the interception.

Unlike these terminal constraints of the interception and impact angle, the look angle constraint is not guaranteed by the convergence of S because it should be satisfied during the entire homing as shown in (4.4d). To confirm whether the proposed guidance law in (4.13) achieves the look angle constraint in (4.4d), the magnitude of the look angle σ_M is investigated as follows

Theorem 4.1. *For all initial conditions satisfying $|\sigma_M(0)| \leq \sigma_M^d$, the look angle is bounded during the entire homing as follows:*

$$|\sigma_M(t)| \leq \sigma_M^{\max} \ \forall t \in [0, t_f]. \tag{4.17}$$

Proof. Let us consider the compact set $\mathbb{B} \triangleq \{\sigma_M : |\sigma_M| \leq \sigma_M^{\max}\}$ for the proof. From (4.13), the dynamics of σ_M under the proposed guidance law is expressed as

$$\begin{aligned}
\dot{\sigma_M} =& \frac{a_M}{V_M} - \dot{\lambda} \\
=& \dot{\sigma}_M^d - k_2 \mathrm{sgn}\,(S) \\
=& k_1 \frac{d}{de_1} \left\{ \mathrm{sat}\left(\frac{e_1}{\phi_1} \right) \right\} \dot{e}_1 - k_2 \mathrm{sgn}\,(S) \\
=& -\frac{k_1 V_M \sin \sigma_M}{R} \frac{d}{de_1} \left\{ \mathrm{sat}\left(\frac{e_1}{\phi_1} \right) \right\} - k_2 \mathrm{sgn}\,(S)\,.
\end{aligned} \tag{4.18}$$

Then, on $\sigma_M = \sigma_M^{\max}$, taking the time derivative of σ_M gives

$$\dot{\sigma}_M\Big|_{\sigma_M=\sigma_M^{\max}} = -\frac{k_1 V_M \sin\sigma_M^{\max}}{R}\frac{d}{de_1}\left\{\mathrm{sat}\left(\frac{e_1}{\phi_1}\right)\right\} - k_2\mathrm{sgn}\left(\sigma_M^{\max} - \sigma_M^d\right). \tag{4.19}$$

Since $d\left\{\mathrm{sat}\left(e_1/\phi_1\right)\right\}/de_1 = 1/\phi_1$ if $|e_1| \leq \phi_1$ and $d\left\{\mathrm{sat}\left(e_1/\phi_1\right)\right\}/de_1 = 0$ otherwise, we obtain

$$\begin{aligned}\dot{\sigma}_M\Big|_{\sigma_M=\sigma_M^{\max}} &\leq -k_2\mathrm{sgn}\left(\sigma_M^{\max} - \sigma_M^d\right)\\ &= -k_2\mathrm{sgn}\left(\sigma_M^{\max} - k_1\mathrm{sat}\left(\frac{e_1}{\phi_1}\right)\right)\\ &\leq 0\end{aligned} \tag{4.20}$$

where the property $0 < k_1 \leq \sigma_M^{\max}$ in (4.8) is used. In a similar way, on $\sigma_M = -\sigma_M^{\max}$, we have

$$\begin{aligned}\dot{\sigma}_M\Big|_{\sigma_M=-\sigma_M^{\max}} &= \frac{k_1 V_M \sin\sigma_M^{\max}}{R}\frac{d}{de_1}\left\{\mathrm{sat}\left(\frac{e_1}{\phi_1}\right)\right\} - k_2\mathrm{sgn}\left(-\sigma_M^{\max} - \sigma_M^d\right)\\ &\geq k_2\mathrm{sgn}\left(\sigma_M^{\max} + \sigma_M^d\right)\\ &\geq 0.\end{aligned} \tag{4.21}$$

The results of (4.20) and (4.21) verifies that $\mathbb{B}$ is an invariant set, which proves (4.17). □

Theorem 4.1 indicates that the look angle is bounded within the prescribed limit during the entire homing. As a result, the guidance law in (4.13) achieves that the missile intercepts the target at the desired impact angle without violating the look angle constraint.

4.3 Impact angle and time control guidance law with look angle constraint

Note that the desired tasks in (4.4a), (4.4b) and (4.4d) are achieved regardless of the magnitude of ϕ_1 which determines the look angle profile as shown in (4.7). It means that the entire trajectory and time-to-go under the developed law can be adjusted as desired by selecting an appropriate value for ϕ_1. Based on this property, remaining time-to-go is calculated in subsection 4.3.1, and an impact angle and time control guidance law is designed using the time-to-go calculation in subsection 4.3.2.

4.3.1 Calculation of time-to-go

In our formulation where the missile flies at a constant speed, the remaining time-to-go at the current time is calculated as follows:

$$t_{go} = \frac{L}{V_M} = \frac{1}{V_M} \int_{final}^{current} dL \tag{4.22}$$

where L is the remaining flight path of the missile. Since the flight path and relative range vary over time as $dL/dt = -V_M$ and $dR/dt = -V_M \cos\sigma_M$ respectively, the time-to-go in (4.22) is expressed as

$$t_{go} = \frac{1}{V_M} \int_{R_f=0}^{R} \sec\sigma_M d\tilde{R} \tag{4.23}$$

for $\tilde{R} \in [0, R]$. After the convergence of S, from (4.7) and (4.10), σ_M in (4.23) is obtained as

$$\sigma_M(\tilde{R}) = \begin{cases} k_1 & \text{for } \left|e_1(\tilde{R})\right| > \phi_1 \quad (4.24a) \\ \sin^{-1}\left\{\alpha(R_1)\tilde{R}^{\beta}\right\} & \text{for } \left|e_1(\tilde{R})\right| \leq \phi_1 \quad (4.24b) \end{cases}$$

where

$$\alpha(R_1) = \sin\left(\frac{k_1}{\phi_1} e_1(R_1)\right) \frac{1}{R_1^{\beta}}, \quad \beta = \frac{k_1}{\phi_1} \tag{4.25}$$

and R_1 in (4.24) and (4.25) is the relative range at $e_1(R) = \phi_1$ and calculated as follows from (4.10a):

$$R_1 = R_0 \exp\left(\frac{\phi_1 - e_1(R_0)}{\tan k_1}\right) \tag{4.26}$$

Now, let us calculate the time-to-go by substituting (4.24) into (4.23). First, when $|e_1(R)| > \phi_1$, the condition of $|e_1(R)| > \phi_1$ is equivalent to $R > R_1$ since $|e_1(R)|$ is monotone increasing for R from (4.10). Thus, the time-to-go when $|e_1(R)| > \phi_1$ is rewritten as

$$t_{go}(R) = \frac{1}{V_M} \int_{R_1}^{R} \sec \sigma_M d\tilde{R} + \frac{1}{V_M} \int_{R_f}^{R_1} \sec \sigma_M d\tilde{R}. \tag{4.27}$$

Substituting (4.24) into (4.27) yields

$$\begin{aligned} t_{go}(R) =& \frac{1}{V_M} \int_{R_1}^{R} \sec k_1 d\tilde{R} + \frac{1}{V_M} \int_{R_f}^{R_1} \frac{1}{\sqrt{1 - \sin^2 \sigma_M(\tilde{R})}} d\tilde{R} \\ =& \frac{\sec k_1}{V_M} (R - R_1) + \frac{1}{V_M} \int_{0}^{R_1} \frac{1}{\sqrt{1 - \alpha^2 (R_1) \tilde{R}^{2\beta}}} d\tilde{R} \end{aligned} \tag{4.28}$$

The second term in (4.28) is rewritten as

$$\frac{1}{V_M} \int_{0}^{R_1} \frac{1}{\sqrt{1 - \alpha^2 (R_1) \tilde{R}^{2\beta}}} d\tilde{R} = \frac{R_1}{2\beta (\sin k_1)^{1/\beta} V_M} \int_{0}^{R_1} \frac{2\beta (\sin k_1)^{1/\beta}}{R_1 \sqrt{1 - \alpha^2 (R_1) \tilde{R}^{2\beta}}} d\tilde{R} \tag{4.29}$$

By using a parameter η defined as $\eta = \alpha^2(R_1)\tilde{R}^{2\beta} = \sin^2 k_1 \left(\tilde{R}/R_1\right)^{2\beta}$, we have

$$\begin{aligned}
\frac{1}{V_M}\int_0^{R_1} \frac{1}{\sqrt{1-\alpha^2\left(R_1\right)\tilde{R}^{2\beta}}} d\tilde{R} =& \frac{R_1}{2\beta\left(\sin k_1\right)^{1/\beta} V_M}\int_0^{\eta(R_1)} \frac{\left(\sin k_1\right)^{1/\beta}\tilde{R}}{R_1\eta\sqrt{1-\eta}} d\eta \\
=& \frac{R_1}{2\beta\left(\sin k_1\right)^{1/\beta} V_M}\int_0^{\eta(R_1)} \frac{1}{\eta\sqrt{1-\eta}}\left(\sin^2 k_1 \frac{\tilde{R}^{2\beta}}{R_1^{2\beta}}\right)^{\frac{1}{2\beta}} d\eta \\
=& \frac{R_1}{2\beta\left(\sin k_1\right)^{1/\beta} V_M}\int_0^{\eta(R_1)} \frac{\eta^{1/2\beta}}{\eta\sqrt{1-\eta}} d\eta \\
=& \frac{R_1}{2\beta\left(\sin k_1\right)^{1/\beta} V_M} B\left(\eta(R_1); \frac{1}{2\beta}, \frac{1}{2}\right) \\
=& \frac{R_1}{2\beta\left(\sin k_1\right)^{1/\beta} V_M} B\left(\sin^2 k_1; \frac{1}{2\beta}, \frac{1}{2}\right)
\end{aligned} \tag{4.30}$$

where $B\left(\cdot;\cdot,\cdot\right)$ is the incomplete beta function. As a result, t_{go} when $|e_1(R)| > \phi_1$ is calculated as

$$\begin{aligned}
t_{go} =& \frac{\sec k_1}{V_M}(R-R_1) + \frac{R_1}{2\beta\left(\sin k_1\right)^{1/\beta} V_M} B\left(\sin^2 k_1; \frac{1}{2\beta}, \frac{1}{2}\right) \\
=& \frac{\sec k_1}{V_M}(R-R_1) + \frac{R_1\phi_1}{2k_1\left(\sin k_1\right)^{\phi_1/k_1} V_M} B\left(\sin^2 k_1; \frac{\phi_1}{2k_1}, \frac{1}{2}\right)
\end{aligned} \tag{4.31}$$

When $|e_1(R)| \leq \phi_1$, the time-to-go is given by

$$t_{go}(R) = \frac{1}{V_M}\int_{R_f}^{R} \sec\sigma_M d\tilde{R}. \tag{4.32}$$

Applying a calculation technique similar to (4.28) $\sim$ (4.31) into (4.32), the time-to-go when $|e_1(R)| \leq \phi_1$ can be obtained as follows:

$$\begin{aligned}
t_{go} =& \frac{R}{2\beta\left|\sin\sigma_M\right|^{1/\beta} V_M} B\left(\sin^2\sigma_M; \frac{1}{2\beta}, \frac{1}{2}\right) \\
=& \frac{R\phi_1}{2k_1\left|\sin\left(\frac{k_1}{\phi_1}e_1\right)\right|^{\phi_1/k_1} V_M} B\left(\sin^2\left(\frac{k_1}{\phi_1}e_1\right); \frac{\phi_1}{2k_1}, \frac{1}{2}\right)
\end{aligned} \tag{4.33}$$

To sum up, the time-to-go under the guidance law in (4.13) is calculated as

$$t_{go} = \begin{cases} \dfrac{\sec k_1}{V_M}(R - R_1) + \dfrac{R_1 \phi_1}{2k_1 (\sin k_1)^{\phi_1/k_1} V_M} B\left(\sin^2 k_1; \dfrac{\phi_1}{2k_1}, \dfrac{1}{2}\right) & \text{for } |e_1(R)| > \phi_1 \quad (4.34a) \\ \dfrac{R\phi_1}{2k_1 \left|\sin\left(\frac{k_1}{\phi_1} e_1\right)\right|^{\phi_1/k_1} V_M} B\left(\sin^2\left(\dfrac{k_1}{\phi_1} e_1\right); \dfrac{\phi_1}{2k_1}, \dfrac{1}{2}\right) & \text{for } |e_1(R)| \leq \phi_1 \quad (4.34b) \end{cases}$$

which is also expressed by using the series as

$$t_{go} = \begin{cases} \dfrac{\sec k_1}{V_M}(R - R_1) + \dfrac{R_1}{V_M} \displaystyle\sum_{n=0}^{\infty} \dfrac{(2n)!}{2^{2n}\left(1 + 2n\frac{k_1}{\phi_1}\right)(n!)^2} \sin^{2n} k_1 & \text{for } |e_1(R)| > \phi_1 \quad (4.35a) \\ \dfrac{R}{V_M} \displaystyle\sum_{n=0}^{\infty} \dfrac{(2n)!}{2^{2n}\left(1 + 2n\frac{k_1}{\phi_1}\right)(n!)^2} \sin^{2n}\left(\dfrac{k_1}{\phi_1} e_1\right) & \text{for } |e_1(R)| \leq \phi_1 \quad (4.35b) \end{cases}$$

Ignoring the higher order term after $\sin^{2n}(\cdot)$ and applying the approximation of $\sin\left(\frac{k_1}{\phi_1} e_1\right) \approx \frac{k_1}{\phi_1} e_1$, the approximated time-to-go is obtained as

$$t_{go} = \begin{cases} \dfrac{\sec k_1}{V_M}(R - R_1) + \dfrac{R_1}{V_M}\left(1 + \dfrac{\sin^2 k_1}{2\left(1 + 2\frac{k_1}{\phi_1}\right)}\right) & \text{for } |e_1(R)| > \phi_1 \quad (4.36a) \\ \dfrac{R}{V_M}\left(1 + \dfrac{\left(\frac{k_1}{\phi_1} e_1\right)^2}{2\left(1 + 2\frac{k_1}{\phi_1}\right)}\right) & \text{for } |e_1(R)| \leq \phi_1. \quad (4.36b) \end{cases}$$

Note that the estimated time-to-go in (4.36) is controllable by adjusting the value of ϕ_1. Based on this property, a proper value for ϕ_1 is found in next subsection 4.3.2 for the impact time control.

4.3.2 Impact time control based on time-to-go calculation

In the previous subsection 4.3.1, it was verified that the time-to-go under the proposed guidance law is a function of the parameter ϕ_1. To achieve the impact time constraint,

therefore, the process to find a proper value of ϕ_1 is investigated in this subsection.

ϕ_1 that guarantees the impact time control can be obtained by solving the following equation:

$$\begin{aligned} t_{go}\left(\phi_1\right) =& t_{go}^{des} \\ \triangleq& t_d - t \end{aligned} \tag{4.37}$$

Since the time-to-go t_{go} has two different expressions depending on the values of e_1 and ϕ_1 as shown in (4.36), the process to calculate the solution of ϕ_1 for the impact time control can be complicated. To simplify the process, the following theorem is introduced.

Theorem 4.2. *Consider $t_{go,1}(\phi_1)$ and $t_{go,2}(\phi_1)$ defined as*

$$t_{go,1}(\phi_1) = \frac{R}{V_M}\left(1 + \frac{\left(\frac{k_1}{\phi_1}e_1\right)^2}{2\left(1+2\frac{k_1}{\phi_1}\right)}\right) \qquad \text{for all } \phi_1 > 0 \tag{4.38}$$

$$t_{go,2}(\phi_1) = \begin{cases} \frac{\sec k_1}{V_M}(R - R_1) + \frac{R_1}{V_M}\left(1 + \frac{\sin^2 k_1}{2\left(1+2\frac{k_1}{\phi_1}\right)}\right) & \text{for } 0 < \phi_1 < |e_1| \\ \frac{R}{V_M}\left(1 + \frac{\left(\frac{k_1}{\phi_1}e_1\right)^2}{2\left(1+2\frac{k_1}{\phi_1}\right)}\right) & \text{for } \phi_1 \geq |e_1| \end{cases} \tag{4.39}$$

Let ϕ_1^* and ϕ_1^{**} be the solutions of $t_{go,1}(\phi_1) = t_{go}^{des}$ and $t_{go,2}(\phi_1) = t_{go}^{des}$ respectively. Then ϕ_1^* and ϕ_1^{**} satisfy $sat\left(e_1/\phi_1^*\right) = sat\left(e_1/\phi_1^{**}\right)$.

Proof. First, let us investigate the solution ϕ_1^* prior to the proof. From (4.38), the solutions satisfying $t_{go,1}(\phi_1^*) = t_{go}^{des}$ is obtained as

$$\phi_1^* = \begin{cases} \dfrac{k_1 R e_1^2}{2\left(V_M t_{go}^{des} - R\right) + \sqrt{4\left(V_M t_{go}^{des} - R\right)^2 + 2Re_1^2\left(V_M t_{go}^{des} - R\right)}} & \text{(4.40a)} \\ \dfrac{k_1 R e_1^2}{2\left(V_M t_{go}^{des} - R\right) - \sqrt{4\left(V_M t_{go}^{des} - R\right)^2 + 2Re_1^2\left(V_M t_{go}^{des} - R\right)}}. & \text{(4.40b)} \end{cases}$$

The solution in (4.40b) satisfies

$$
\begin{aligned}
&\frac{k_1 R e_1^2}{2\left(V_M t_{go}^{des}-R\right)-\sqrt{4\left(V_M t_{go}^{des}-R\right)^2+2Re_1^2\left(V_M t_{go}^{des}-R\right)}} \\
=&\frac{k_1 R e_1^2}{2\left|V_M t_{go}^{des}-R\right|\left(\operatorname{sgn}\left(V_M t_{go}^{des}-R\right)-\sqrt{1+\frac{Re_1^2}{2\left(V_M t_{go}^{des}-R\right)}}\right)} \\
\leq&0,
\end{aligned}
\tag{4.41}
$$

which implies that more than one solution for ϕ_1^* cannot exist.

Now, let us prove the theorem in two cases: $0 < \phi_1^* < |e_1|$ and $\phi_1^* \geq |e_1|$. First, if $0 < \phi_1^* < |e_1|$, the solution satisfying $\phi_1^* \geq |e_1|$ does not exist by the result of (4.40) and (4.41). Then, ϕ_1^{**} satisfying $\phi_1^{**} \geq |e_1|$ also does not exist because $t_{go,1}(\phi_1) = t_{go,2}(\phi_1)$ when $\phi_1 \geq |e_1|$. Consequently, the solution ϕ_1^{**} also satisfies $0 < \phi_1^{**} < |e_1|$ when $0 < \phi_1^* < |e_1|$.

If $\phi_1^* \geq |e_1|$, it is obvious that the solution ϕ_1^{**} is obtained as $\phi_1^{**} = \phi_1^* \geq |e_1|$ since $t_{go,1}(\phi_1) = t_{go,2}(\phi_1)$ when $\phi_1 \geq |e_1|$ as shown in (4.38) and (4.39). As a result, ϕ_1^* and ϕ_1^{**} satisfy $\operatorname{sat}(e_1/\phi_1^*) = \operatorname{sat}(e_1/\phi_1^{**})$ in both cases. □

When the guidance law in (4.13) is implemented, the parameter ϕ_1 is used to compose σ_M^d as a form of $\operatorname{sat}(e_1/\phi_1)$, which is shown in (4.7). Therefore, Theorem 4.2 signifies that solving the equation $t_{go,1}(\phi_1) = t_{go}^{des}$ is sufficient to obtain the solution of ϕ_1 satisfying (4.37) for the implementation of the proposed guidance law. The solutions of $t_{go,1}(\phi_1) = t_{go}^{des}$ are given by (4.40), and (4.41) in Theorem 4.2 reveals that the solution in (4.40b) is invalid since it is proved as negative. Therefore, we have the substantive solution as

$$
\phi_1 = \frac{k_1 R e_1^2}{2\left(V_M t_{go}^{des}-R\right)+\sqrt{4\left(V_M t_{go}^{des}-R\right)^2+2Re_1^2\left(V_M t_{go}^{des}-R\right)}}. \tag{4.42}
$$

That is, choosing the parameter ϕ_1 as (4.42) enables the impact time control.

4.4 Numerical simulation

In this section in which two subsections are included, the validity of the proposed guidance law is demonstrated through numerical simulations. In subsection 4.4.1, the proposed law is simulated for various engagement scenarios to evaluate the performance. In subsection 4.4.2, the proposed law is compared with other guidance laws that consider the impact angle and time constraints.

The signum function $\mathrm{sgn}\,(\cdot)$ in (4.13) can cause the command chattering due to its discontinuity. To alleviate the fluctuation and obtain a continuous feasible guidance command, the signum function is approximated as the following hyperbolic tangent function in the implementation.

$$\tanh\,(ax) = \frac{2}{1+\exp^{-2ax}} - 1 \tag{4.43}$$

where the value of a is chosen as $a = 10$. The approximation of (4.43) allows the convergence of S to be achieved by a continuous command with a deviation inversely proportional to a from the ideal siding mode [44]. In all the scenarios of the following simulations, the homing is performed until the relative range is less than or equal to 0.5 m, and the guidance command of the missile is saturated at $\pm 10\ g$. The detailed setting of the parameters used in the simulations are listed in Table 4.1.

Table 4.1: Simulation setting

Parameters	Values
Initial position of the missile $(x_M(0), y_M(0))$	$(0, 0)$ km
Position of the stationary target $(x_T(0), y_T(0))$	$(10, 0)$ km
Initial missile flight path angle $\gamma_M(0)$	30 deg
Missile speed V_M	250 m/s
Missile acceleration limits $\lvert a_M \rvert^{\max}$	$10\ g^{\dagger}$
Guidance gains	$k_1 = \sigma_M^{\max} - 0.01,\ k_2 = 1$

† g denotes the gravitational acceleration, i.e., $g = 9.81$ m/s^2.

4.4.1 Performance analysis of the proposed guidance law

To investigate the performance of the proposed law, four scenarios where the terminal impact angle and time are constrained as $(\gamma_d, t_d) = (-30°, 45\,s)$, $(-45°, 50\,s)$, $(-90°, 60\,s)$, and $(-120°, 65\,s)$ respectively with setting the look angle limitation as $\sigma_M^{\max} = 60°$ are considered. Figures 4.2a $\sim$ 4.2d illustrates the simulation results of the four scenarios under the proposed guidance law.

Figure 4.2a shows that the proposed law fulfills the interception against the stationary target for every case. Specifically, the proposed law achieves the impact angles and times of $(\gamma_M(t_f), t_f) = (-29.96°, 44.99\text{ s})$, $(-44.98°, 49.99\text{ s})$, $(-89.98°, 59.99\text{ s})$ and $(-119.97°, 64.99\text{ s})$ in the four scenarios respectively. This result means that the impact angle and time errors are within 0.04° and 0.01 s respectively for all the scenarios.

Figure 4.2b shows that the proposed guidance law makes the surface variable S converge to zero with generating the command that does not exceed $\pm 10\ g$. At the early stage of the homing in every case, the guidance law yields a relatively large acceleration, which is due to the demand that achieves the sliding mode. After the convergence of S, there also exists an interval where the command slightly decreases in every case. It is related with a sudden decrease of σ_M which can be found in Fig. 4.2d.

Figure 4.2c provides the histories of impact angle and time errors, i.e. e_1 in (4.5) and $t_{go} - t_{go}^{des}$ respectively. The exact solution for the time-to-go in (4.34) is used as t_{go}. First, it is observed that e_1 converges to zero as the missile approaches the target in every scenario, which accords with the theoretical result in (4.10). The second row of Fig. 4.2c shows that the impact time error also goes to zero before the end of the homing. Since the proposed law uses the approximate time-to-go in (4.36) to satisfy the impact time constraint, the accuracy of the impact time control is not always ensured during the entire homing. This is why there is a difference between t_{go} and t_{go}^{des} at the early and middle stages of the homing. However, as e_1 converges to zero, the difference between the exact time-to-go in (4.34) and the approximate one in (4.36) also becomes zero. Therefore, the convergence of the impact

time error to zero is guaranteed at the end of the homing, which can be seen in the second row of Fig. 4.2c.

Figure 4.2d presents the histories of the flight path angle and look angle of the missile in each scenario. The first row of Fig. 4.2d confirms that the proposed guidance law satisfies the impact angle constraint in all scenarios like Fig. 4.2c. The second row of Fig. 4.2d demonstrates that the look angle does not violate the prescribed limit $\sigma_M^{\max} = 60°$, which accords with the theoretical verification of Theorem 4.1. In summary, the proposed law enables the missile to intercept the stationary target at the desired impact angle and time without violating the pre-set field-of-view limit.

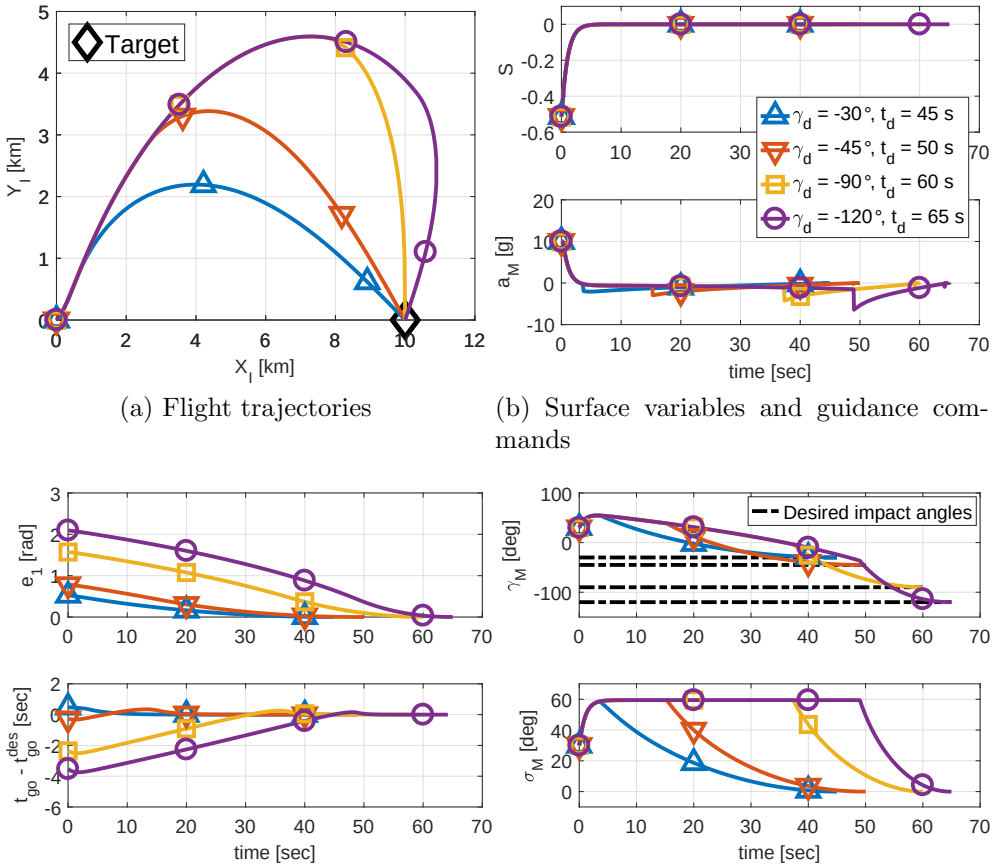

(a) Flight trajectories

(b) Surface variables and guidance commands

(c) Impact angle and time errors

(d) Flight path angles and look angles

Figure 4.2: Simulation results under the proposed guidance law

4.4.2 Performance comparison with other guidance laws in realistic scenarios

This subsection compares the proposed guidance law with another guidance law that is able to control the terminal impact angle and time called MPG (multi-phase guidance law) studied in [39]. MPG can be applied to the missile with limited FOV due to its ability to confine the look-angle within the prescribed limit. However, MPG is vulnerable to unexpected disturbances and uncertainties because control of the impact angle and time is carried out as an open-loop process.

For the comparative analysis of the proposed guidance law with the existing law, this subsection considers three scenarios where a large detour is required to satisfy the desired impact angle and time with the presence of three different disturbances. All of three scenarios are aimed at achieving the desired impact angle and time of $\gamma_d = -80°$ and $t_d = 50$ s respectively with the look angle limitation of $\sigma_M^{\max} = 45°$. A first-order transfer function is applied between the guidance command and engagement dynamics to take into account the autopilot delay, and the time constant of the transfer function is set to be 0.2. In addition, considering the aerodynamics, gravitation, and controllable thrust, the missile speed and flight path angle are assumed to vary with

$$\dot{V}_M = \frac{T - D}{m} - g \sin \gamma_M + \Delta \tag{4.44}$$

$$\dot{\gamma}_M = \frac{a_M - g \cos \gamma_M}{V_M}. \tag{4.45}$$

where T, D, m, and Δ represent the longitudinal thrust force, aerodynamic drag, missile mass, and disturbance caused by a longitudinal wind gust. The mass is fixed as $m = 90$ kg and the drag model used in [26, 51] is adopted to formulate D in our simulation. The

disturbance is modeled differently for each scenario as follows:

$$\Delta = \begin{cases} 0 & \text{for the scenario \#1} \\ +g\left\{H(t) - H(t-10)\right\} & \text{for the scenario \#2} \\ -g\left\{H(t) - H(t-10)\right\} & \text{for the scenario \#3} \end{cases} \tag{4.46}$$

where $H(\cdot)$ is the Heaviside step function; i.e., the gust influences for the first 10 seconds in the scenarios #2 and 3. The thrust is assumed to be controllable to maintain the desired speed $V_M^d = 250$ m/s as

$$T = T_{eq} + K_P\left(V_M^d - V_M\right) \tag{4.47}$$

where T_{eq} is the equivalent thrust force to maintain the speed in an ideal condition and K_P is the proportional gain selected as $K_P = 30$.

The simulation results with the speed-varying model described above are illustrated in Figs. 4.3 $\sim$ 4.5 and also summarized in Table 4.2. Figures 4.3, 4.4, and 4.5 provide the results in the scenarios #1, 2, and 3 respectively. Figs. 4.3a, 4.4a, and 4.5a show that both laws achieve the interception in all the scenarios. In addition, as shown in the lower row of Figs. 4.3b $\sim$ 4.5b, MPG and the proposed law prevent the look-angle from exceeding the prescribed limit $\sigma_M^{\max} = 45°$ during the entire homing although a curved trajectory is demanded to satisfy the terminal constraints on impact angle and time. Thus, both MPG and the proposed law can be applied when the missile is equipped with the seeker with reduced FOV.

The results in Table 4.2 also show that the proposed law produces smaller impact angle and time errors than MPG in every scenario. MPG achieves the interception for every case but does not ensure accurate impact angle and time. It is because MPG is vulnerable to uncertainties and disturbances due to the absence of a feedback process to regulate the impact angle and time errors as described in [39]. The results of the scenario #2 and 3

clearly show the performance degradation of MPG caused by disturbances. In the scenario #2, the missile under MPG intercepts the target 1.433 s faster than the desired impact time because the wind accelerates the missile during the first 10 seconds as shown in Fig. 4.4c. The opposite result arises in the scenario #3; the missile intercepts the target 0.947 s later than the requirement.

Unlike MPG, the proposed law ensures the precise impact angle and time control with satisfying $|\gamma_M(t_f) - \gamma_d| \leq 0.02°$ and $|t_f - t_d| \leq 0.001\,\text{s}$. The reason for the performance difference between MPG and the proposed law is as follows. MPG calculates the parameters to satisfy the desired impact angle and time based on initial conditions, which is classified as the open-loop control. On the contrary, the proposed law has the feedback loop to regulate the impact angle and time errors e_1 and $t_{go} - t_{go}^{des}$ based on current state variables as shown in (4.7) and (4.42), which is the closed-loop control. For this reason, the proposed law yields better performance than MPG in the presence of disturbances. As a result, the proposed law can guarantee better performance for various impact angle and time conditions in real applications compared with the existing guidance law.

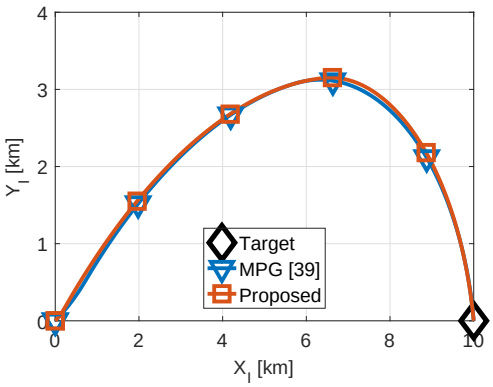

(a) Flight trajectories in the scenario #1

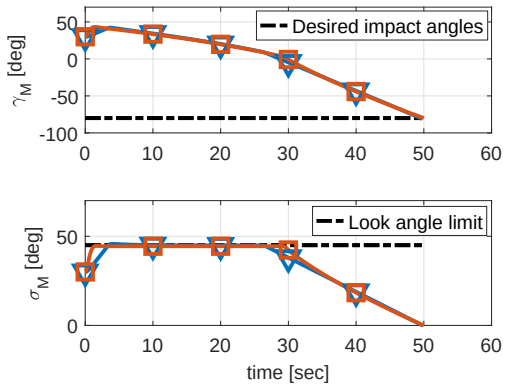

(b) Flight path angles and look angles in the scenario #1

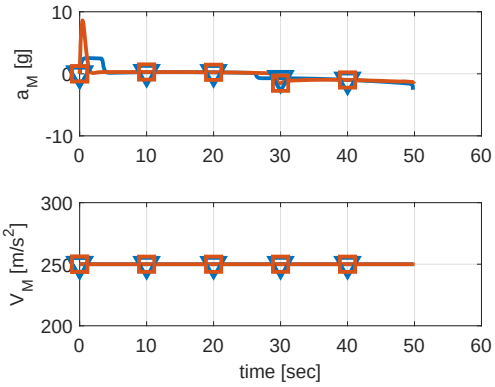

(c) Lateral accelerations and speeds in the scenario #1

Figure 4.3: Simulation results in the scenario #1 under two guidance laws: MPG and the proposed law

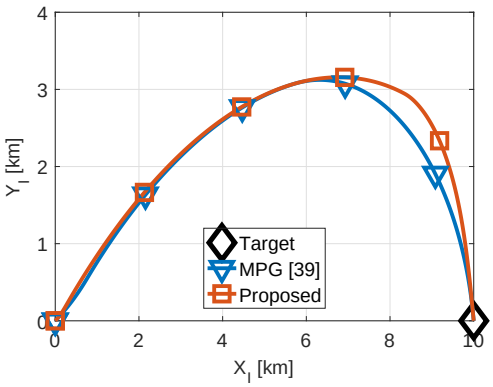

(a) Flight trajectories in the scenario #2

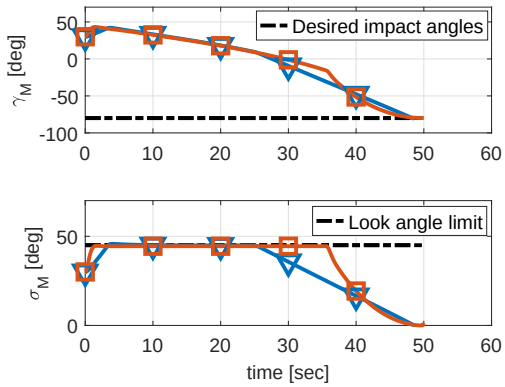

(b) Flight path angles and look angles in the scenario #2

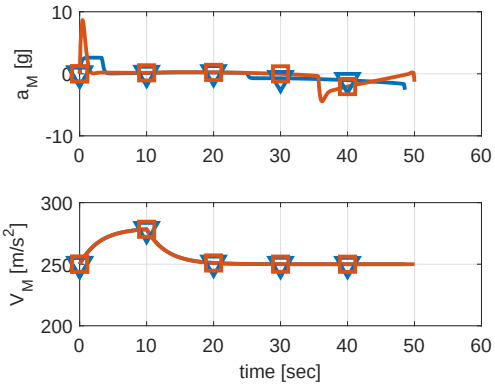

(c) Lateral accelerations and speeds in the scenario #2

Figure 4.4: Simulation results in the scenario #2 under two guidance laws: MPG and the proposed law

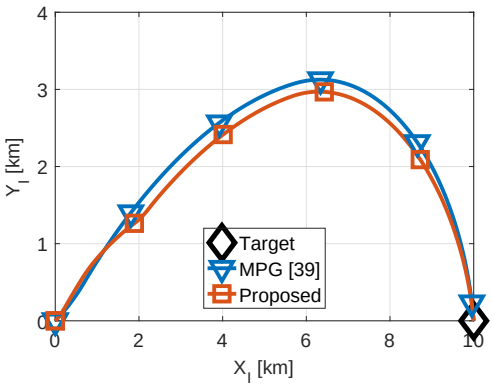

(a) Flight trajectories in the scenario #3

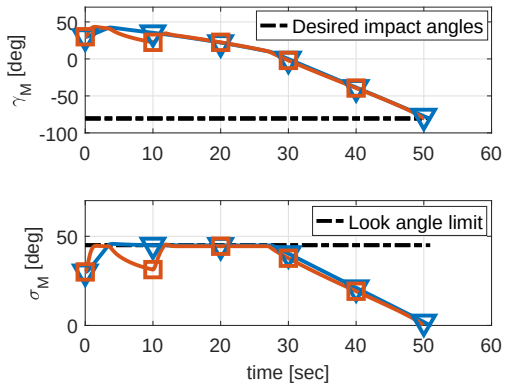

(b) Flight path angles and look angles in the scenario #3

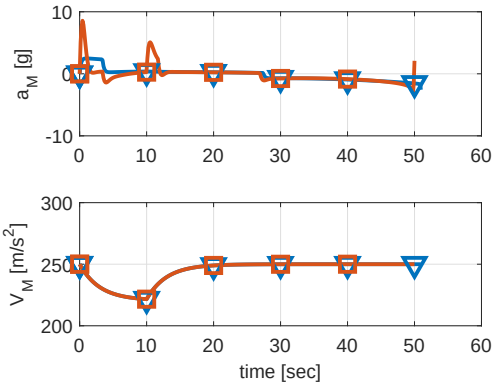

(c) Lateral accelerations and speeds in the scenario #3

Figure 4.5: Simulation results in the scenario #3 under two guidance laws: MPG and the proposed law

Table 4.2: Summarized results of the simulation

Scenario	Guidance law	Miss distance $R(t_f)$ [m]	Impact angle error $\gamma_M(t_f) - \gamma_d$ [deg]	Impact time error $t_f - t_d$ [sec]
1	MPG	0.394	-1.198	-0.242
	Proposed	**0.389**	**-0.009**	**-0.001**
2	MPG	0.391	-1.133	-1.433
	Proposed	**0.378**	**0.017**	**-0.001**
3	MPG	0.401	-1.239	0.947
	Proposed	**0.268**	**0.015**	**-0.001**

5

Conclusions

In this dissertation, guidance laws for missiles with reduced field-of-view constraint are proposed in each part composed of the following: (*i*) impact angle control guidance, (*ii*) impact time control guidance, and (*iii*) impact angle and time control guidance. Each part verifies that each proposed guidance law ensures the interception of a stationary target without violating the prescribed field-of-view constraint while achieving the design objective of each part through the theoretical analysis and the numerical simulations. The main results of each study are summarized as:

- The look angle-constrained impact angle control guidance law that only uses the bearing angles among the target information is proposed. To develop the guidance law, the surface variable that only consists of the line-of-sight angle and look angle is designed based on the kinematic conditions for achieving the impact angle constraint with confining the missile look angle within the pre-specified limit. The guidance law is derived to achieve the sliding mode of the defined surface variable. Since imposing the terminal impact angle constraint requires the curved trajectory, this capability to prevent the missile look angle from exceeding the prescribed limit is helpful from a

practical standpoint. Furthermore, unlike the existing laws whose implementation demands the knowledge of the relative range or line-of-sight rate, the proposed guidance law only needs the line-of-sight angle and look angle among the target information. Hence, the proposed law can easily be implemented into a homing missile equipped with a structurally simple passive strapdown seeker. Both the theoretical analysis and the numerical simulation result indicate that the proposed guidance law achieves the desired tasks under bearings-only measurements.

- The impact time control guidance law considering the seeker's field-of-view limits is investigated. The proposed guidance law is motivated by the fact that implementation of an impact time control guidance requires the consideration of the seeker's field-of-view limits due to its curved trajectory. To take into account the impact time control problem, the kinematic conditions are introduced, and the guidance law is designed in order to satisfy the conditions based on the backstepping control technique. In the control structure, the magnitude of the missile look angle is confined within a prescribed range by restricting the controller gain, which allows the seeker's field-of-view to be within specific limits as a result. Numerical simulation result demonstrates that the proposed law allows the missile to intercept the target at the desired impact time without violating the seeker's field-of-view limits.

- The look angle constrained guidance law that is able to achieve the interception at the desired impact angle and time is presented. The look angle profile that guarantees the constraints on the desired impact angle and time is designed, and the guidance law is structured to follow the designed look angle profile using the sliding mode control method. Since the look angle profile is constructed to be smaller than the prescribed limit, the proposed guidance law can ensure the terminal impact angle and time conditions while preventing the look angle from exceeding the specified limit. Owing to this capability to obey the look angle constraint, the proposed law can easily be implemented to a homing missile equipped with a narrow field-of-view. In addition, the

proposed approach fulfills the impact angle and time control through state feedback structure, so more accurate performance is expected in real applications compared with the existing approach based on open-loop structure. Numerical simulations are performed and the results confirm that the proposed law yields satisfactory performance despite the presence of disturbances.

References

[1] P. Zarchan, *Tactical and Strategic Missile Guidance*, 5th ed. Reston, VA: AIAA, Inc., 2007.

[2] A. E. Bryson and Y. C. Ho, *Applied Optimal Control*. Washington, DC: Hemisphere, 1975.

[3] M. Kim and K. V. Grider, "Terminal guidance for impact attitude angle constrained flight trajectories," *IEEE Transactions on Aerospace and Electronic Systems*, vol. 9, no. 6, pp. 852–859, 1973.

[4] M. Idan, O. M. Golan, and M. Guelman, "Optimal planar interception with terminal constraints," *Journal of Guidance, Control, and Dynamics*, vol. 18, no. 6, pp. 1273–1279, 1995.

[5] B. S. Kim, J. G. Lee, and H. S. Han, "Biased png law for impact with angular constraint," *IEEE Transactions on Aerospace and Electronic Systems*, vol. 34, no. 1, pp. 277–288, 1998.

[6] T. L. Song and S. J. Shin, "Time-optimal impact angle control for vertical plane engagements," *IEEE Transactions on Aerospace and Electronic Systems*, vol. 35, no. 2, pp. 738–742, 1999.

[7] C. K. Ryoo, H. Cho, and M. J. Tahk, "Optimal guidance laws with terminal impact angle constraint," *Journal of Guidance, Control, and Dynamics*, vol. 28, no. 4, pp. 724–732, 2005.

[8] M.-G. Yoon, "Relative circular navigation guidance for the impact angle control problem," *IEEE Transactions on Aerospace and Electronic Systems*, vol. 44, no. 4, pp. 1449–1463, 2008.

[9] S. R. Kumar, S. Rao, and D. Ghose, "Sliding-mode guidance and control for all-aspect interceptors with terminal angle constraints," *Journal of Guidance, Control and Dynamics*, vol. 35, no. 4, pp. 1230–1246, 2012.

[10] ——, "Nonsingular terminal sliding mode guidance with impact angle constraints," *Journal of Guidance, Control, and Dynamics*, vol. 37, no. 4, pp. 1114–1130, 2014.

[11] D. Cho, H. J. Kim, and M.-j. Tahk, "Impact angle constrained sliding mode guidance against maneuvering target with unknown acceleration," *IEEE Transactions on Aerospace and Electronic Systems*, vol. 51, no. 2, pp. 1310–1323, 2015.

[12] C. H. Lee, T. H. Kim, M. J. Tahk, and I. H. Whang, "Polynomial guidance laws considering terminal impact angle and acceleration constraints," *IEEE Transactions on Aerospace and Electronic Systems*, vol. 49, no. 1, pp. 74–92, 2013.

[13] T.-H. Kim, C.-H. Lee, and M.-J. Tahk, "Time-to-go polynomial guidance with trajectory modulation for observability enhancement," *IEEE Transactions on Aerospace and Electronic Systems*, vol. 49, no. 1, pp. 55–73, 2013.

[14] B.-G. Park, T.-H. Kim, and M.-J. Tahk, "Optimal impact angle control guidance law considering the seeker's field-of-view limits," *Proceedings of the Institution of Mechanical Engineers, Part G: Journal of Aerospace Engineering*, vol. 227, no. 8, pp. 1347–1364, 2013.

[15] ——, "Range-to-go weighted optimal guidance with impact angle constraint and seeker's look angle limits," *IEEE Transactions on Aerospace and Electronic Systems*, vol. 52, no. 3, pp. 1241–1256, 2016.

[16] K. S. Erer and O. Merttopcuoglu, "Indirect impact-angle-control against stationary targets using biased pure proportional navigation," *Journal of Guidance, Control, and Dynamics*, vol. 35, no. 2, pp. 700–704, 2012.

[17] K. S. Erer, R. Tekin, and M. K. Ozgoren, "Look angle constrained impact angle control based on proportional navigation," in *AIAA Guidance, Navigation, and Control Conference*, 2015, pp. 2015–0091.

[18] T.-H. Kim, B.-G. Park, and M.-J. Tahk, "Bias-shaping method for biased proportional navigation with terminal-angle constraint," *Journal of Guidance, Control, and Dynamics*, vol. 36, no. 6, pp. 1810–1816, 2013.

[19] R. Tekin and K. S. Erer, "Switched-gain guidance for impact angle control under physical constraints," *Journal of Guidance, Control, and Dynamics*, vol. 38, no. 2, pp. 205–216, 2015.

[20] A. Ratnoo, "Analysis of two-stage proportional navigation with heading constraints," *Journal of Guidance, Control, and Dynamics*, vol. 39, no. 1, pp. 156–164, 2016.

[21] A. Ratnoo and D. Ghose, "Impact angle constrained interception of stationary targets," *Journal of Guidance, Control, and Dynamics*, vol. 31, no. 6, pp. 1816–1821, 2008.

[22] ——, "Impact angle constrained guidance against nonstationary nonmaneuvering targets," *Journal of Guidance, Control, and Dynamics*, vol. 33, no. 1, pp. 269–275, 2010.

[23] I. S. Jeon, J. I. Lee, and M. J. Tahk, "Impact-time-control guidance law for anti-ship missiles," *IEEE Transactions on Control Systems Technology*, vol. 14, no. 2, pp. 260–266, 2006.

[24] ——, "Homing guidance law for cooperative attack of multiple missiles," *Journal of Guidance, Control, and Dynamics*, vol. 33, no. 1, pp. 275–280, 2010.

[25] M. Kim, B. Jung, B. Han, S. Lee, and Y. Kim, "Lyapunov-based impact time control guidance laws against stationary targets," *IEEE Transactions on Aerospace and Electronic Systems*, vol. 51, no. 2, pp. 1111–1122, 2015.

[26] S. R. Kumar and D. Ghose, "Impact time guidance for large heading errors using sliding mode control," *IEEE Transactions on Aerospace and Electronic Systems*, vol. 51, no. 4, pp. 3123–3138, 2015.

[27] D. Cho, H. J. Kim, and M.-J. Tahk, "Nonsingular sliding mode guidance for impact time control," *Journal of Guidance, Control, and Dynamics*, vol. 39, no. 1, pp. 61–68, 2016.

[28] N. Cho and Y. Kim, "Modified pure proportional navigation guidance law for impact time control," *Journal of Guidance, Control, and Dynamics*, vol. 39, no. 4, pp. 852–872, 2016.

[29] A. Saleem and A. Ratnoo, "Lyapunov-based guidance law for impact time control and simultaneous arrival," *Journal of Guidance, Control, and Dynamics*, vol. 39, no. 1, pp. 164–172, 2016.

[30] I.-S. Jeon, J.-I. Lee, and M.-J. Tahk, "Impact-time-control guidance with generalized proportional navigation based on nonlinear formulation," *Journal of Guidance, Control, and Dynamics*, vol. 39, no. 8, pp. 1885–1890, 2016.

[31] D. Sang and M. Tahk, "Guidance law switching logic considering the seeker's field-of-view limits," *Proceedings of the Institution of Mechanical Engineers, Part G: Journal of Aerospace Engineering*, vol. 223, no. 8, pp. 1049–1058, 2009.

[32] Y. Zhang, X. Wang, and H. Wu, "Impact time control guidance law with field of view constraint," *Aerospace Science and Technology*, vol. 39, pp. 361–369, 2014.

[33] ——, "Impact time control guidance with field-of-view constraint accounting for uncertain system lag," *Proceedings of the Institution of Mechanical Engineers, Part G: Journal of Aerospace Engineering*, vol. 230, no. 3, pp. 515–529, 2016.

[34] I.-S. Jeon and J.-I. Lee, "Impact-time-control guidance law with constraints on seeker look angle," *IEEE Transactions on Aerospace and Electronic Systems*, 2017.

[35] J. I. Lee, I. S. Jeon, and M. J. Tahk, "Guidance law to control impact time and angle," *IEEE Transactions on Aerospace and Electronic Systems*, vol. 43, no. 1, pp. 301–310, 2007.

[36] T. H. Kim, C. H. Lee, I. S. Jeon, and M. J. Tahk, "Augmented polynomial guidance with impact time and angle constraints," *IEEE Transactions on Aerospace and Electronic Systems*, vol. 49, no. 4, pp. 2806–2817, 2013.

[37] N. Harl and S. N. Balakrishnan, "Impact time and angle guidance with sliding mode control," *IEEE Transactions on Control Systems Technology*, vol. 20, no. 6, pp. 1436–1449, 2012.

[38] S. Arita and S. Ueno, "Optimal feedback guidance for nonlinear missile model with impact time and angle constraints," in *AIAA Guidance, Navigation, and Control (GNC) Conference*, vol. 4785, 2013.

[39] K. S. Erer and R. Tekin, "Impact time and angle control based on constrained optimal solutions," *Journal of Guidance, Control, and Dynamics*, vol. 39, no. 10, pp. 2445–2451, 2016.

[40] S.-W. Shim, S.-M. Hong, G.-H. Moon, and M.-J. Tahk, "Impact angle and time control guidance under field-of-view constraints and maneuver limits," *International Journal of Aeronautical & Space Sciences*, vol. 19, no. 1, pp. 217–226, 2018.

[41] A. BRYSON, JR and J. Speyer, "Optimal programming problems with a bounded state space." *AIAA journal*, vol. 6, no. 8, pp. 1488–1491, 1968.

[42] H.-G. Kim, J.-Y. Lee, and H. J. Kim, "Look angle constrained impact angle control guidance law for homing missiles with bearings-only measurements," *IEEE Transactions on Aerospace and Electronic Systems*, Accepted for publication.

[43] Y. Shtessel, C. Edwards, L. Fridman, and A. Levant, *Sliding mode control and observation*. Springer, 2014.

[44] V. Utkin, J. Guldner, and J. Shi, *Sliding mode control in electro-mechanical systems*. CRC press, 2009, vol. 34.

[45] T. Shima, M. Idan, and O. M. Golan, "Sliding-mode control for integrated missile autopilot guidance," *Journal of guidance, control, and dynamics*, vol. 29, no. 2, pp. 250–260, 2006.

[46] H.-G. Kim and H. J. Kim, "Impact time control guidance considering seeker's field-of-view limits," in *Decision and Control (CDC), 2016 IEEE 55th Conference on*. IEEE, 2016, pp. 4160–4165.

[47] ——, "Backstepping-based impact time control guidance law for missiles with reduced seeker field-of-view," *IEEE Transactions on Aerospace and Electronic Systems*, Accepted for publication.

[48] G. M. Siouris, *Missile guidance and control systems*. Springer Science & Business Media, 2004.

[49] D. Swaroop, J. K. Hedrick, P. P. Yip, and J. C. Gerdes, "Dynamic surface control for a class of nonlinear systems," *IEEE transactions on automatic control*, vol. 45, no. 10, pp. 1893–1899, 2000.

[50] W. Rudin, "Principles of mathematical analysis (international series in pure & applied mathematics)," 1976.

[51] P. Kee, L. Dong, and C. Siong, "Near optimal midcourse guidance law for flight vehicle," in *36th AIAA Aerospace Sciences Meeting and Exhibit*, 1998, p. 583.

국 문 초 록

호밍 유도 법칙이란 유도탄에 탑재된 탐색기로부터 얻은 정보를 이용하여 지정된 표적으로의 유도를 수행하는 일련의 기법들을 지칭한다. 호밍 유도 법칙의 실제 적용에 있어 표적 조준 유지는 유도 정보 획득을 위해 필수적이며, 이를 위해서는 탐색기의 시야 제한을 고려하여 유도 법칙을 설계하는 것이 중요하다. 특히, 충돌각 및 충돌시간 제어 유도법칙의 구현시에는 큰 곡률을 가지는 비행궤적이 필요하여 유도탄의 비행방향이 표적으로부터 크게 벗어날 가능성이 높아지기 때문에 탐색기의 시야각 제한 고려는 더욱 필수적이다.

본 논문에서는 탐색기의 시야각 제한을 고려한 i) 충돌각 제어 유도, ii) 충돌시간 제어 유도, iii) 충돌각 및 충돌시간 제어 유도의 세 법칙을 제안한다.

첫째, 탐색기의 시야 제한을 고려한 충돌각 제어 유도 법칙을 제안한다. 슬라이딩 모드를 만족하면 요구 충돌각으로 정지 표적에 대한 호밍이 수행되도록 슬라이딩 변수를 정의하고, 제안한 변수가 슬라이딩 평면에 도달하도록 유도 법칙을 설계한다. 출력의 크기를 제한하는 시그모이드 함수를 슬라이딩 변수 설계에 활용함으로써, 제안한 유도 법칙은 표적에 대한 지향각을 제한하면서 충돌각 제어와 호밍 유도를 수행한다. 충돌각 제어는 유도탄의 곡선궤적을 야기하고 지향각은 표적에 대한 시야를 결정하므로, 제안 유도 법칙은 탐색기의 시야가 제한적인 상황에 유용하다. 또한, 제안한 유도 법칙은 구현시에 시선각 및 지향각 정보만을 필요로 하기 때문에, 구조적으로 간단한 스트랩다운 탐색기가 부착된 유도탄에 쉽게 적용할 수 있다.

둘째, 다수 유도탄의 일제 동시 공격을 위한 충돌시간 제어 및 탐색기의 시야 제한 또한 고려한 유도 법칙을 제안한다. 표적 요격 및 충돌시간 구속조건에 대한 운동학 기반 조건을 정의하고, 백스테핑 제어를 이용하여 정의한 조건을 만족하도록 유도 법칙을 설계한다. 제안한 백스테핑 제어 기반 유도 법칙은 유도탄의 지향각을 가상 제어 입력으로 이용하며, 시그모이드 함수를 이용하여 가상 제어 입력의 크기를 제한한다. 결과적으로, 설계된 유도 법칙은 시야각 제한을 위반하지 않음과 동시에 충돌시간 구속조건을 만족하도록 호밍을 수행한다. 충돌각 제어와 마찬가지로 충돌시간 제어도 유도탄의 표적에 대한 지향각의 증가를

야기하므로, 제안한 충돌시간 유도 법칙 또한 탐색기의 시야가 제한적인 상황에 유용하다.

마지막으로, 탐색기의 시야 제한을 고려하며 보다 효과적인 다수 유도탄의 일제 동시 공격을 가능하게 하는 충돌각 및 충돌시간 제어 유도 법칙을 제안한다. 제안 유도 법칙은 기본적으로 시야 제한을 고려한 충돌각 유도법칙의 형태로 설계되며, 추가적인 제어 이득을 갖도록 구성된다. 제안한 법칙 하에서 유도탄의 궤적이 추가 제어 이득의 함수로 계산되기 때문에, 적절한 값을 계산하여 제어 이득으로 선택함으로써 충돌시간의 제어 또한 가능하다. 결과적으로, 제안 법칙은 시야 제한을 위반하지 않으며 충돌각 및 충돌시간 제어를 수행할 수 있다. 설계한 유도 법칙은 오프라인 최적화 등의 수치 계산을 필요로 하지 않으며 상태 변수의 피드백에 기반한 폐루프 구조이기 때문에, 실제 적용 상황에 있어 개루프 구조의 기존 기법에 비해 보다 정확한 성능이 기대된다.

제안한 유도 법칙들의 성능 평가를 위해 각 법칙에 대해 수치 시뮬레이션을 수행하였으며, 시뮬레이션 결과는 제안한 법칙들 모두 탐색기의 시야 제한 조건을 위반하지 않으며 각 요구 구속조건들을 충족함을 보여준다.

주요어: 호밍 유도, 시야각 제한, 충돌각 제어, 충돌시간 제어

학　번: 2014-30356